Journal of
Medicinal Chemistry

Article

Identification of Diketopiperazine-Containing 2-Anilinobenzamides as Potent Sirtuin 2 (SIRT2)-Selective Inhibitors Targeting the "Selectivity Pocket", Substrate-Binding Site, and NAD-Binding Site

Paolo Mellini, Yukihiro Itoh, Elghareeb E. Elboray, Hiroki Tsumoto, Ying Li, Miki Suzuki, Yukari Takahashi, Toshifumi Tojo, Takashi Kurohara, Yuka Miyake, Yuri Miura, Yuki Kitao, Masayuki Kotoku, Tetsuya Iida, and Takayoshi Suzuki

J. Med. Chem., **Just Accepted Manuscript** • DOI: 10.1021/acs.jmedchem.9b00255 • Publication Date (Web): 30 May 2019

Just Accepted

is published by the American Chemical Society. 1155 Sixteenth Street N.W., Washington, DC 20036

Identification of Diketopiperazine-Containing 2-Anilinobenzamides as Potent Sirtuin 2 (SIRT2)-Selective Inhibitors Targeting the "Selectivity Pocket", Substrate-Binding Site, and NAD^+-Binding Site

Paolo Mellini,[†] Yukihiro Itoh,[†] Elghareeb E. Elboray,[†,‡] Hiroki Tsumoto,[#] Ying Li,[†] Miki Suzuki,[†] Yukari Takahashi,[†] Toshifumi Tojo,[†] Takashi Kurohara,[†] Yuka Miyake,[†] Yuri Miura,[#] Yuki Kitao,[†] Masayuki Kotoku,[†] Tetsuya Iida,[†] and Takayoshi Suzuki[,†,§]*

[†]Graduate School of Medical Science, Kyoto Prefectural University of Medicine, 1-5 Shimogamohangi-cho, Sakyo-ku, Kyoto, 606-0823, Japan

[‡]Chemistry Department, Faculty of Science, South Valley University, Qena, 83523, Egypt

[#]Research Team for Mechanism of Aging, Tokyo Metropolitan Institute of Gerontology, 35-2 Sakae-cho, Itabashi-ku, Tokyo 173-0015, Japan

[§]CREST, Japan Science and Technology Agency (JST), 4-1-8 Honcho Kawaguchi, Saitama 332-0012, Japan

ABSTRACT

The NAD^+-dependent deacetylase SIRT2 represents an attractive target for drug development. Here, we designed and synthesized drug-like SIRT2-selective inhibitors based on an analysis of the putative binding modes of recently reported SIRT2-selective inhibitors, and evaluated their SIRT2-inhibitory activity. This led us to develop a more drug-like diketopiperazine structure as a "hydrogen bond (H-bond) hunter" to target the substrate-binding site of SIRT2. Thioamide **53**, a conjugate of diketopiperazine and 2-anilinobenzamide which is expected to occupy the "selectivity pocket" of SIRT2, exhibited potent SIRT2-selective inhibition. Inhibition of SIRT2 by **53** was mediated by the formation of a **53**-ADP-ribose conjugate, suggesting that **53** is a mechanism-based inhibitor targeting the "selectivity pocket", substrate-binding site, and NAD^+-binding site. Furthermore, **53** showed potent antiproliferative activity towards breast cancer cells and promoted neurite outgrowth of Neuro-2a cells. These findings should pave the way for the discovery of novel therapeutic agents for cancer and neurological disorders.

INTRODUCTION

Since the discovery of Sir2 in *S. cerevisae* in 1979 by Klar and co-workers,[1] the biological function of sirtuins (SIRT1–7)[2] has been widely investigated. Sirtuins were originally identified as NAD^+-dependent lysine deacetylases of histone and non-histone proteins,[3,4] but recent studies have revealed that their catalytic activity is not limited to deacetylation. Sirtuins also efficiently catalyze the hydrolysis of *N*ε-acyl lysines such as long-chain fatty acyl (SIRT1–3, 6, and 7),[5–7] 4-oxononanonyl (SIRT2),[8] succinyl (SIRT5), and benzoyl lysines (SIRT2).[9–11] These findings, together with the different subcellular compartmentalizations of the isotypes,[12] highlight that sirtuins have key roles in regulating multiple biological processes. To date, the activities of SIRT1, 3, and 6 have been linked to metabolic functions such as mitochondrial biogenesis, fatty acid oxidation, cholesterol efflux, insulin secretion, and glucose homeostasis.[13,14] SIRT1 inhibits lipid accumulation through inhibition of PPARγ activity[15] and participates in the control of glucose metabolism by deacetylation of PGC1-α[16,17] and repression of UCP2[18]. SIRT3 is highly expressed in metabolically active tissues such as skeletal muscle, brain, liver, and heart.[19,20] It is involved in energy production and exerts antioxidant effects via deacetylation of AceCS2,[21,22] SOD2,[23,24] and IDH2.[25] SIRT6 regulates glucose homeostasis via GLUT1 inhibition and promotes expression of glycolytic genes, functioning as a HIF1-α co-repressor.[26–28] Among sirtuins, SIRT2 is most highly expressed in brain.[29,30] Its genetic or pharmacological inhibition is associated with neuroprotection in models of both Parkinson's and Huntington diseases;[31–36] especially, treatment of the models of Parkinson's and Huntington's diseases with small-molecular SIRT2 inhibitors was found to be effective in reducing α-synuclein-mediated toxicity and polyglutamine inclusions.[33–36] Furthermore, a potential link between inhibition of SIRT2 activity and antidepressant-like action has recently been revealed by

Tordera and co-workers.[37] Thus, SIRT2 is interesting as a therapeutic target for neurological disorders.

The role of SIRT1 and 2 in cancer progression is controversial.[38–42] In normal cells, SIRT1 promotes genomic stability. In some cancer cells, SIRT1 has been reported to promote cell survival through deacetylation of p53, followed by silencing of tumor suppressor HIC1.[43,44] In addition, SIRT1-suppression by miR34a induces apoptosis of cancer cells.[45] In contrast, SIRT1 acts as a tumor suppressor via HIF1-α,[46] leading to inhibition of tumor growth and vascular formation. Accordingly, it is still unclear whether activation or inhibition of SIRT1 is beneficial. The functions of SIRT2 are thought to be highly dependent on cancer type. For example, a study on SIRT2-deficient mice suggests that SIRT2 acts as a tumor suppressor in liver.[47] On the other hand, other studies on patient samples, biochemical pathway analysis, and small molecular SIRT2 inhibitors suggest that SIRT2 acts as a tumor promoter in acute myeloid leukemia,[48,49] prostate cancer,[50] and neuroblastoma.[51] Accordingly, pharmacological inhibition of SIRT2 is effective on certain specific cancers.

Many SIRT inhibitors have been reported.[52–54] SIRT1 and 2 inhibitors such as salermide,[55] tenovin-6,[56,57] and AC-93523[58] (Chart1) showed interesting anticancer properties when tested against a panel of cancer cells, including cancer stem cells, but their low inhibitory potency combined with non-optimal isotype selectivity made it difficult to predict their biological activity. Currently, chroman-4-ones,[59,60] NCO-90,[61,62] 1,2,4-oxadiazoles,[63] thienopyrimidinone,[64] RK-9123016,[65] NPD11033,[66] SirReals,[67–72] and TM[73] have been reported as SIRT2-selective inhibitors (Chart 1). Among them, SirReals and TM have been studied well. SirReal2 inhibits the SIRT2-downstream target PEPCK1, which is associated with mitochondrial metabolism and the RAS/ERK/JNK/MMP-9 pathway, and decreases migration as well as invasion of human gastric cancer cells.[74] TM shows not only

antiproliferative activity towards a large panel of cancer cells including leukemia, non-small cell lung cancer, colon, prostate, and breast cancer cells, but also the ability to discriminate between normal breast cells and cancer cells: the anticancer effects are strictly dependent on SIRT2 inhibition, which leads to time-dependent c-Myc degradation.[73] These findings have put the spotlight back on SIRT2-selective inhibitors as valuable tools to investigate the druggability of SIRT2 in cancers.

We recently developed low-micromolar active, SIRT2-selective inhibitor KPM-1[75] (Chart 1 and Supporting Information, Figure S1a) by molecular fusion of NCO-90 and a pseudopeptidic substrate-mimetic compound. The substitution of the KPM-1 acyl oxygen with sulfur led to KPM-2[75] (Chart 1), a nanomolar SIRT2 mechanism-based inhibitor (Supporting Information Figure S1b) with antiproliferative activity towards breast cancer cells and potent neurite outgrowth activity. In this study, aiming to improve the non drug-like peptide structure of KPM-1 and KPM-2, we explored in detail targeting of the SIRT2 "selectivity pocket", substrate-binding site, and NAD^+-binding site by means of structure-activity relationship studies of NCO-90 bearing a 2-anilinobenzamide moiety. Herein, we report the rational design, synthesis, and biological activity of SIRT2-selective inhibitors based on the 2-anilinobenzamide scaffold.

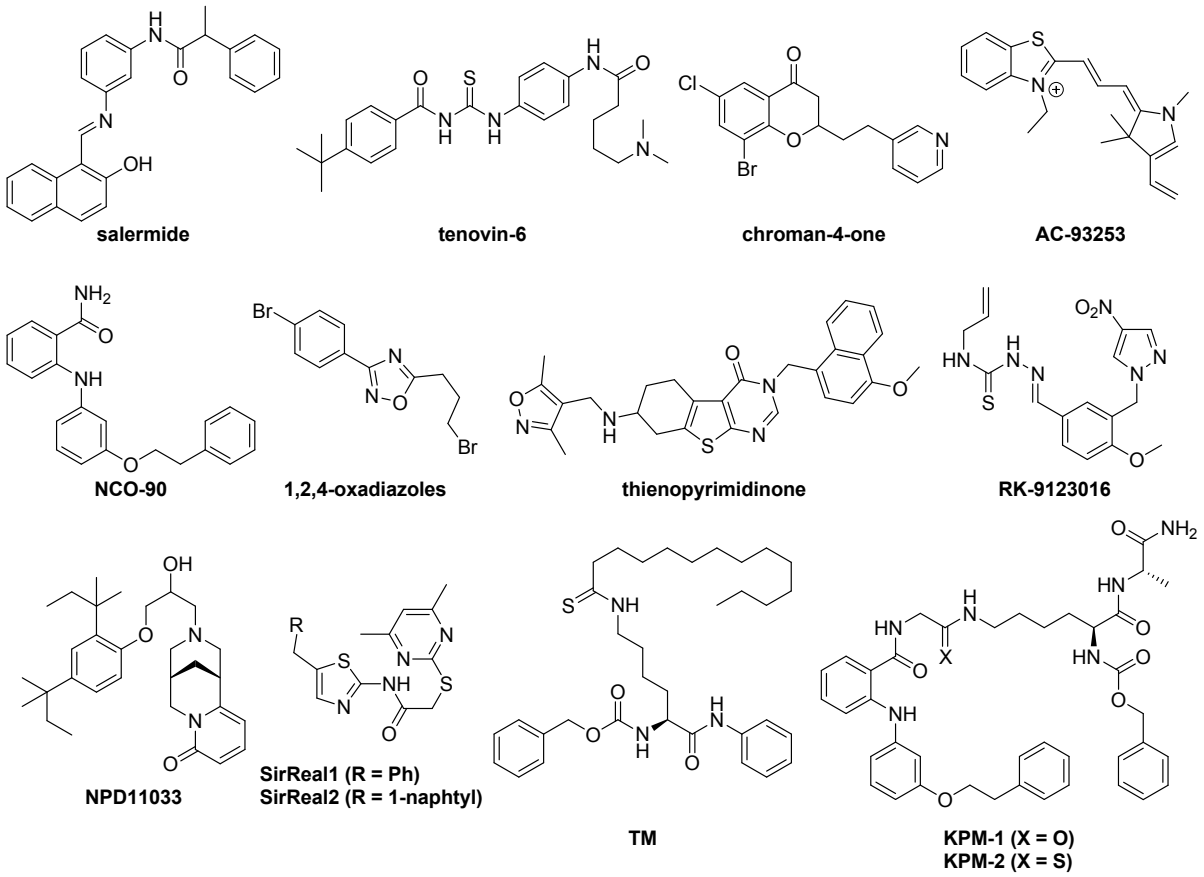

Chart 1. Representative SIRT1 and SIRT2 inhibitors.

RESULTS AND DISCUSSION

Chemistry. Compounds **2**, **3**, **8**, **12**, **18–43**, and **53** were synthesized as shown in Schemes 1–4. The preparation of **2**, **3**, and **8** is illustrated in Scheme 1. Alcohol **1**[61] was etherified with 2-(2-bromoethyl)naphthalene[76] or esterified with 2-[(4,6-dimethylpyrimidin-2-yl)thio]acetic acid[77] in the presence of coupling reagent 1-[(1-(cyano-2-ethoxy-2-oxoethylideneaminooxy) dimethylaminomorpholino)]uronium hexafluorophosphate (COMU)[78] to obtain **2** or **3**, respectively. Compound **8** was synthesized by Buchwald-Hartwig coupling between **4** and **5**, followed by reduction of the nitro group and amidation with 2-[(4,6-dimethylpyrimidin-2-yl)thio]acetic acid.

Scheme 1. Synthesis of compounds **2**, **3**, and **8**.[a]

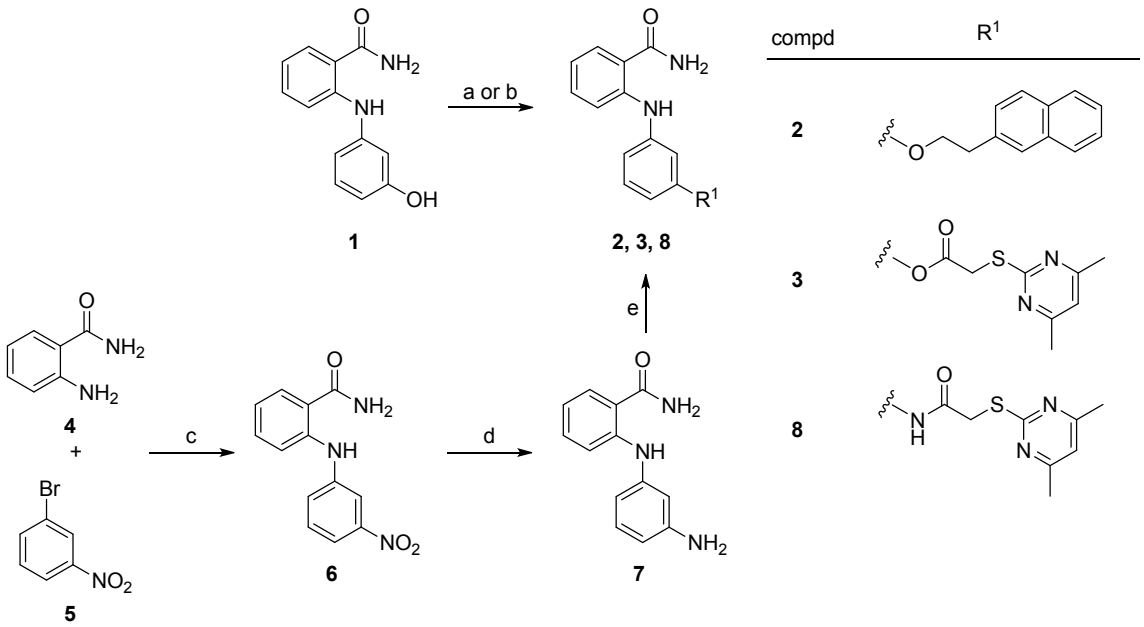

[a]Reagents and conditions: (a) 2-(2-bromoethyl)naphthalene, K_2CO_3, acetone, reflux 18 h (for **2**); (b) 2-[(4,6-dimethylpyrimidin-2-yl)thio]acetic acid, COMU®, Et_3N, DMF, 0°C to rt, 18 h (for **3**); (c) Pd_2dba_3, 2-dicyclohexylphosphino-2',4',6'-triisopropyl biphenyl (XPhos), K_2CO_3, *t*-BuOH, reflux, 18–20 h; (d) Pd/C, H_2, MeOH, 2 h; (e) 2-[(4,6-dimethylpyrimidin-2-yl)thio]acetic acid, EDCI·HCl, HOBt, Et_3N, DMF, 0°C to rt, 17 h.

Scheme 2 shows the synthesis of **12**. Condensation of acid **9** with ammonia afforded amide **10**. Reduction of nitro group of **10** in the presence of Pd/C catalyst yielded amine **11**. Compound **11** was converted to **12** by Buchwald-Hartwig coupling with 1-bromo-3-phenethoxybenzene.[61]

Scheme 2. Synthesis of compound **12**.[a]

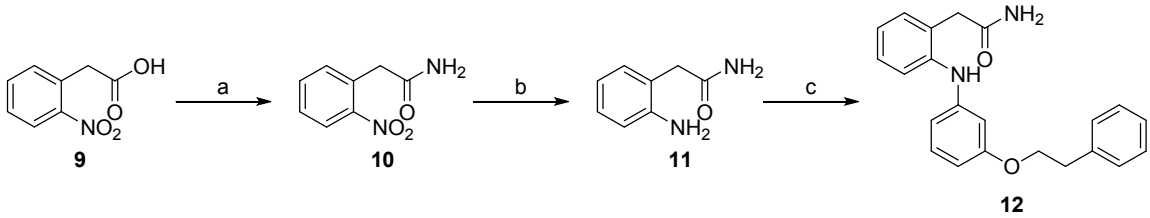

[a]Reagents and conditions: (a) $(COCl)_2$, DMF, CH_2Cl_2, 0°C to rt, 180 min, then NH_3, aqueous solution, THF; (b) Pd/C, H_2, MeOH, 5 h; (c) 1-bromo-3-phenethoxybenzene, Pd_2dba_3, XPhos, K_2CO_3, *t*-BuOH, reflux, 8 h.

Scheme 3 shows the preparation of **19**–**43**. Amine **17**, which was used for the preparation of **43**, was synthesized from **13** in four steps: coupling reaction with glycine ethyl ester, Boc deprotection under acidic conditions, diketopiperazine formation, and Cbz deprotection in the presence of Pd/C catalyst. Compounds **19**–**31** and **33**–**39** were synthesized by coupling reactions using 1-ethyl-3-(3-dimethylaminopropyl)carbodiimide hydrochloride (EDCI·HCl) and 1-hydroxybenzotriazole (HOBt) from the corresponding amines and acid **18**, which was prepared as described previously.[61,75] Hydroxamic acid **32** was prepared by hydrolysis of the tetrahydropyranyl acetal group of **29**. Hydrolysis of ester **39** afforded acid **40**, which was reacted with appropriate amines to afford **41**–**43**.

Scheme 3. Synthesis of compounds **19–43**.[a]

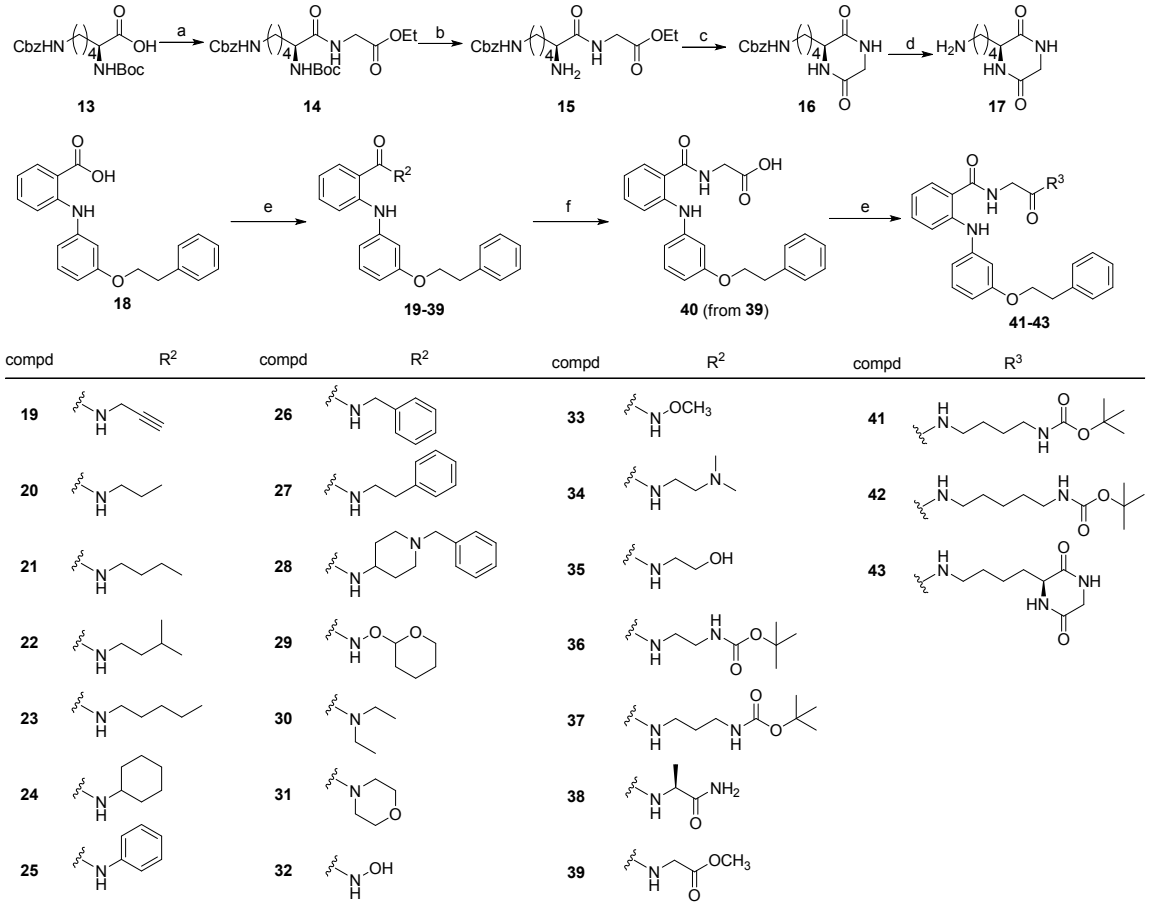

[a]Reagents and conditions: (a) glycine ethyl ester hydrochloride, COMU®, Et_3N, DMF, 0°C to rt, 24 h; (b) CF_3COOH, CH_2Cl_2, rt, overnight; (c) CH_3COOH, *N*-methylmorpholine, 1-butanol, reflux, 220 min; (d) H_2, Pd/C, MeOH, rt, 3 h; (e) corresponding amine, EDCI·HCl, HOBt, Et_3N, CH_2Cl_2, 0°C to rt, 15–17 h; (f) LiOH, THF, MeOH, H_2O, rt, 150 min.

Compound **53** was prepared from **13** (Scheme 4). Methyl esterification and deprotection of the Cbz group of **13** afforded amine **45**. Coupling reaction between **45** and *N*-Fmoc glycine gave **46**, and reaction using Lawesson's reagent[79] efficiently led to **47**. Then, hydrolysis of **47** in the presence of trimethyltin hydroxide[80] and condensation with glycine ethyl ester afforded **49**. Compound **49** was treated with trifluoroacetic acid to furnish **50**. Then, diketopiperazine formation and deprotection of Fmoc group using piperidine were conducted to obtain **52**. Finally, condensation between **18** and **52** furnished the desired compound **53**.

Scheme 4. Synthesis of compound **53**.[a]

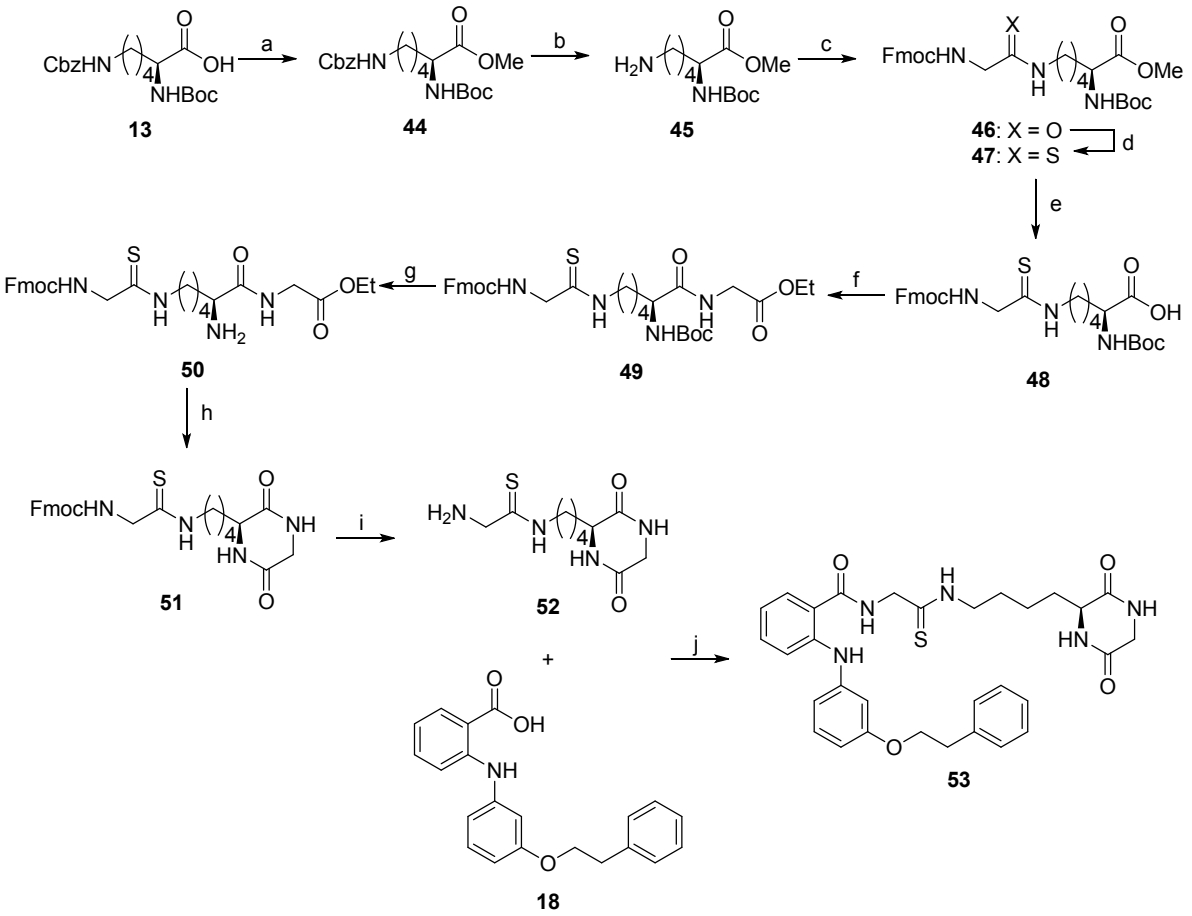

[a]Reagents and conditions: (a) MeI, K_2CO_3, acetone, reflux, 26 h; (b) Pd/C, H_2, MeOH, rt, 3 h; (c) *N*-Fmoc-glycine, COMU®, *i*-Pr_2NEt, DMF, CH_2Cl_2, 0°C to rt, 4 h; (d) Lawesson's reagent, toluene, 60°C, 3 h; (e) Me_3SnOH, $ClCH_2CH_2Cl$, 60°C, 10 h; (f) glycine ethyl ester hydrochloride, COMU®, *i*-Pr_2NEt, DMF, CH_2Cl_2, 0°C to rt, 4 h; (g) CF_3COOH, CH_2Cl_2, 0°C to rt, 2 h; (h) CH_3COOH, NMM, 1-butanol, reflux, 220 min; (i) piperidine, CH_2Cl_2, rt, 30 min; (j) COMU®, *i*-Pr_2NEt, DMF, CH_2Cl_2, 0°C to rt, 3 h.

Design of NCO-90 derivatives and *in vitro* evaluation of inhibitory activity towards SIRT1 and SIRT2. We recently solved the X-ray crystal structure of SIRT2 complexed with NCO-90, which revealed that the inhibitor binds to the "selectivity pocket"[67] where the phenoxyethylphenyl moiety of NCO-90 establishes π-π and CH-π interactions, and the 2-anilinobenzamide core protrudes towards the acetyl-lysine substrate-binding site (Figure 1a,b).[75] Based on this X-ray structure and another structure of SIRT2 complexed with a

pseudopeptide substrate (Figure 1c,d), we previously identified KPM-1 and KPM-2 as SIRT2-selective inhibitors, which were designed by conjugating NCO-90 and a pseudopeptide substrate structure (Figure 1e and Supporting Information Figure S1a,b).[75,81] We also found that introduction of small glycinamide handles into NCO-90 did not affect the SIRT2-inhibitory activity. We assume that glycinamide dislodges a water molecule (HOH4) and forms an H-bonding interaction with Val233 (Figure 1b,d,e) and that potent SIRT2 inhibition was achieved by introduction of the pseudopeptide scaffold, which mimics a lysine residue substrate. We considered that the peptide bonds could interact with Gly236, Glu237, and Gln267 through H-bond formation (Figure 1d,e). In order to provide additional insights into drug-like fragments targeting the binding site of acetyl-lysine substrate, we prepared and screened a new small library of NCO-90 analogues, using SIRT1 and SIRT2 inhibition assays. The naphthyl (**2**) and pyrimidine derivatives (**3** and **8**) were designed to probe the versatility of NCO-90 as a SIRT2 inhibitor scaffold (Figure 1f, part A). The acetamide (**12**), carboxylic acid (**18**) and amides with small/bulky hydrocarbon groups (**19**–**27**) were tested to elucidate the structure-activity relationship of the benzamide moiety, and amides with polar groups (**28**–**40**) were expected to interact directly with Val233 (Figure 1f, part B). Furthermore, compounds **41**–**43** were prepared as "H-bonds hunters" to target Gly236, Glu237, and Gln267 in SIRT2 (Figure 1f, part C). All the compounds prepared in this study were screened in in vitro assays using SIRT1 and SIRT2, and NCO-90 was used as a reference compound (Table 1). The SIRT1-inhibitory activities of the tested compounds were relatively low even at 50 μM (Table 1). Therefore, we focus mainly on the SIRT2-inhibitory activities at 10 μM in the following section.

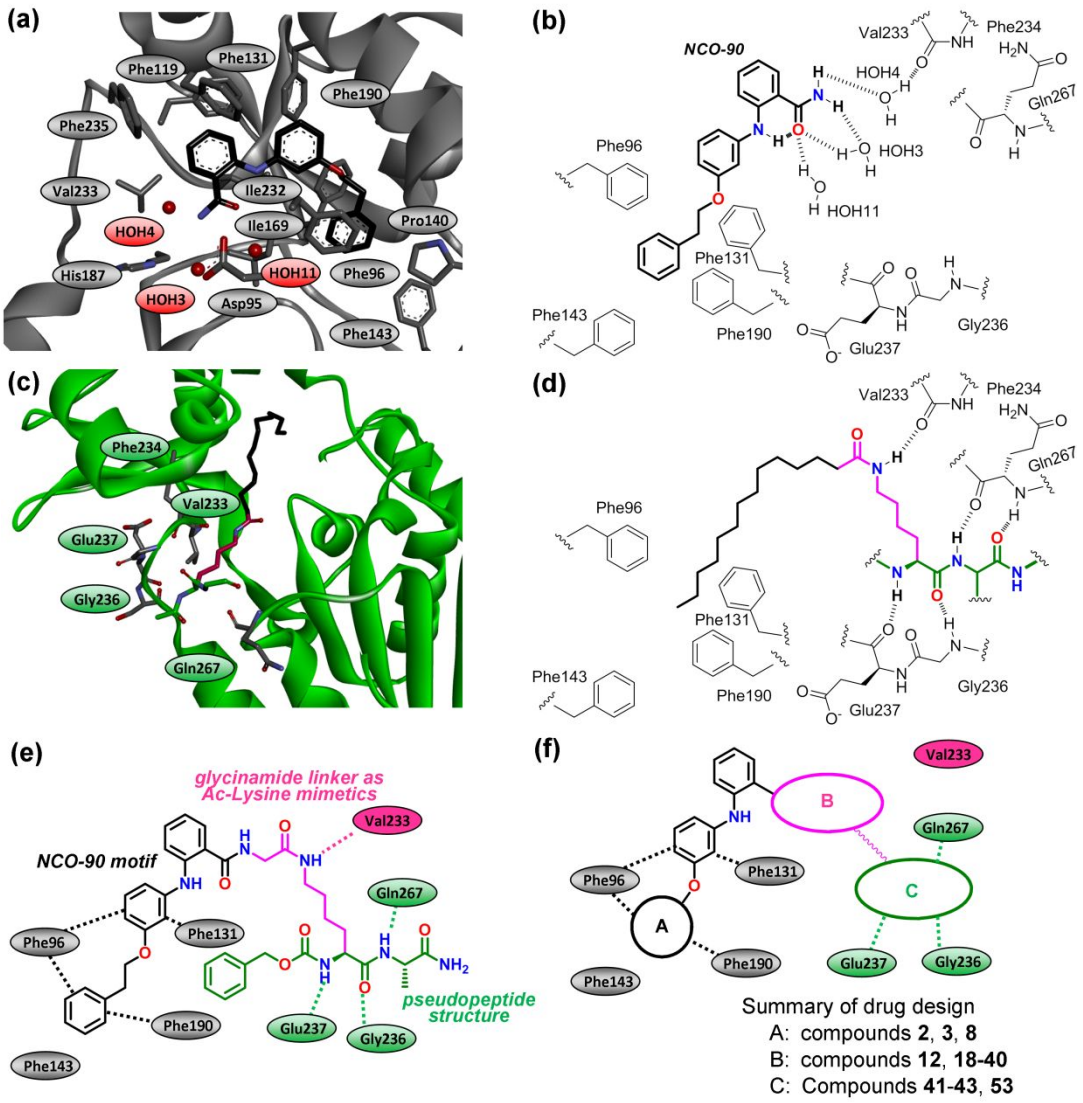

Figure 1. (a) X-ray structure of SIRT2 in the complex with NCO-90 (black) (PDB code: 5Y5N). (b) Schematic diagram of Figure 1a. (c) X-ray structure of SIRT2 in the complex with myristoylated substrate peptide (black, purple, and green) (PDB code: 4Y6O). (d) Schematic diagram of Figure 1c. (e) Plausible binding mode of KPM-1 on SIRT2. NCO-90 motif, glycinamide handle, and pseudopeptide structure of KPM-1 are presented in black, purple, and green, respectively. The π-π and CH-π interactions are represented by black dashed lines, and H-bonds are represented by purple or green dashed lines. (f) Drug design of SIRT2-selective inhibitors.

Table 1. SIRT1 and SIRT2 inhibitory activities of compounds **2**, **3**, **8**, **12**, **18–43**, **53** and **54**.

Cmpd.	% SIRT1 inhibition at 50 μM[a]	% SIRT2 inhibition at 10 μM[a]
NCO-90	12 ± 0.36	90 ± 1.5
2	7 ± 2.2	75 ± 0.2
3	7 ± 0.07	26 ± 2.7
8	16 ± 0.03	93 ± 0.13 47 ± 0.30 (at 1 μM)
12	19 ± 1.0	68 ± 4.2
18	2.5 ± 2.5	12 ± 3.3
19	12 ± 1.3	77 ± 0.01
20	8 ± 0.6	58 ± 0.22
21	2 ± 2.0	57 ± 0.3
22	8 ± 0.06	45 ± 1 70 ± 1.1 (at 50 μM)
23	9 ± 2.1	50 ± 0.33
24	15 ± 2.3	28 ± 0.67
25	9 ± 3.7	44 ± 4.8
26	12 ± 0.6	70 ± 0.92
27	5 ± 0.83	46 ± 0.09
28	8 ± 1	56 ± 0.23
29	8 ± 0.54	54 ± 1.1
30	11 ± 0.41	61 ± 0.95
31	4 ± 0.81	71 ± 0.81
32	13 ± 2.9	68 ± 1.9
33	6 ± 0.06	63 ± 2.7
34	18 ± 1.6	59 ± 1.7 74 ± 0.52 (at 50 μM)
35	12 ± 1.1	76 ± 0.4
36	11 ± 0.41	77 ± 5.6
37	4 ± 0.06	57 ± 2.1
38	15 ± 1	81 ± 0.9
39	17 ± 0.73	72 ± 0.45
40	8 ± 2.6	50 ± 1.3
41	23 ± 0.15	83± 0.25
42	14 ± 0.23	83 ± 1.0
43	9 ± 3.9	92 ± 0.47 59 ± 0.91 (at 1 μM)
53	41 ± 2.1	73 ± 6.8 (at 1 μM)
54	10 ± 1.9[b]	85 ± 0.47[b]

[a]Fluor de Lys assay, values are means ± SD of at least two experiments. [a]Data from ref. 75.

Initially, we tested **2**, **3**, and **8** (Scheme 1), which were designed by modifying the phenyl group of NCO-90. Because the phenyl group of NCO-90 is located at a hydrophobic pocket formed by Phe96, Phe143, and Phe190,[75] we anticipated that more hydrophobic moiety such as a naphthyl group might improve the SIRT2-inhibitory activity. However, the replacement of the phenyl group of NCO-90 with a naphthyl group (**2**) resulted in decreased SIRT2-inhibitory activity (Table 1). We next focused on the superimposition of SIRT2 crystal structures in the complexes with NCO-90 (PDB code: 5Y5N) and SirReal1 (PDB code: 4RMI).[67] The phenyl group and the thiazole ring of SirReal1 are partly superimposable on the 2-anilinobenzamide core (Figure 2). Based on this, we designed **3**, in which the pyrimidine handle of SirReal1 is connected with 2-anilinobenzamide of NCO-90. However, **3** showed only very weak SIRT2 inhibition at 10 μM concentration. We speculated that the ester group of **3** favored an elongated conformation that does not optimally fit in the selectivity pocket. As previously reported by Rumpf et al.,[67] a peculiarity of SirReal2 is the formation of an intramolecular H-bond (Figure 2) that confers conformational rigidity. Such a molecular feature was also expected in NCO-90. Thus, we designed **8**, in which the pyrimidine moiety of SirReal1 is connected with the 2-anilinobenzamide of NCO-90 via amide bond to obtain a new scaffold with two intramolecular H-bonds. One is formed between the amide (-C=O) and aromatic amine (-NH), and the other is formed between the secondary amide (-NH) and nitrogen of the pyrimidine ring (Figure 2). As we expected, compound **8** exhibited similar SIRT2 inhibitory potency to NCO-90 (Table 1).

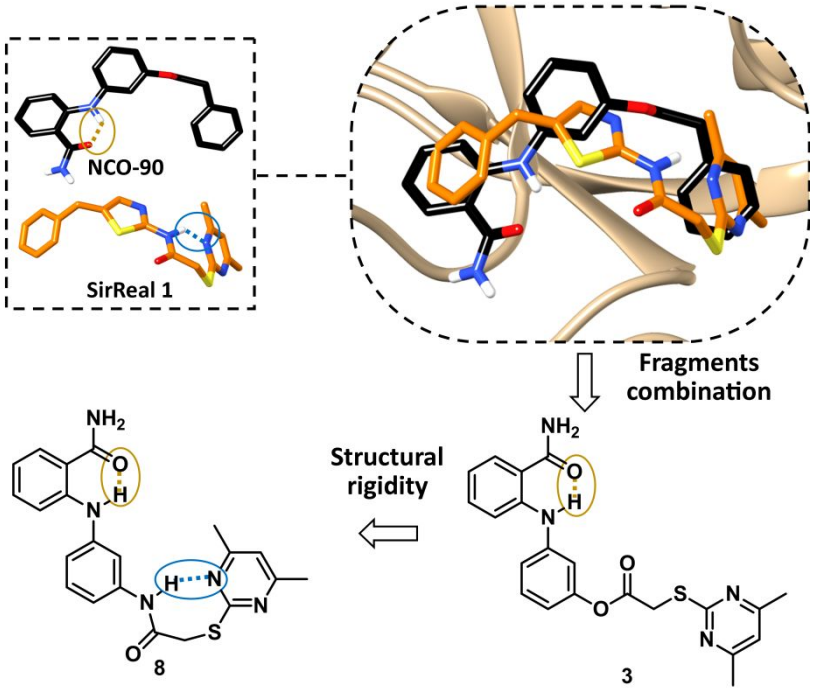

Figure 2. Fragment switching design applied to NCO-90 with compounds **3** and **8** using the pyrimidine moiety of SirReal1. These compounds were designed based on superimposition of the SIRT2/SirReal2 (PDB code: 4RMI) and SIRT2/NCO-90 (PDB code: 5Y5N) crystal structures.

Subsequently, we evaluated compounds **12** (Scheme 2) and **18**–**40** (Scheme 3), aiming to optimize the benzamide part of NCO-90. The switch from aromatic amide of NCO-90 to acetamide (**12**) did not lead to potent inhibition. Amide functionalization with aliphatic amines (**19**–**23**) gave compounds showing 45–77% SIRT2 inhibition. Modeling studies with **21** and **23** (Figure 3a,b) showed that the aliphatic moiety displaces water molecule HOH4, originally located near His187 and Val233 (Figure 1a), and the only interactions were with the water molecules HOH3 and HOH11, which are thought to be weakly bound, because they appear to be displaced upon NAD^+ binding. The cyclohexyl amide derivative (**24**) showed the weakest SIRT2 inhibition (28% inhibition) among the amide compounds. Docking simulations indicate that steric hindrance near the anilinobenzamide core plus ring flexibility might induce a suboptimal binding mode (Figure 3c), which would explain the low inhibitory

activity. When a phenyl ring was introduced instead of the cyclohexyl ring, a slight improvement of SIRT2 inhibition was observed (**25** vs **24**). Introduction of a methylene spacer between the aromatic ring and amide function in benzylamide derivative (**26**) provided greater activity (**26** vs **25**), which might be ascribable to sandwiched π-π and CH-π interaction with His187 and Phe235 (Figure 3d). However, the SIRT2-inhibitory activity was decreased when a longer linker with a phenethylamide was used (**27** vs **26**). Bulky compounds **28** and **29** showed moderate SIRT2 inhibition ≥ 54%, and *N*,*N*-diethylamide (**30**) and morpholine amide (**31**) retained moderate SIRT2-inhibitory activity (61% and 71% inhibition, respectively). The shift from the polar carboxylic acid precursor (**18**) to hydroxamic and methylhydroxamic derivatives (**32** and **33**) increased SIRT2 inhibition to a moderate level. The introduction of a nitrogen atom into the isopentylamide **22** (compound **34**) did not significantly affect SIRT2 inhibition (**22**: 45% at 10 μM, 70% at 50 μM; **34**: 59% at 10 μM, 74% at 50 μM). However, the activity was improved when ethanolamide (**35**) was used as an H-bond donor (**35** vs **22** vs **20**). Docking simulations suggested that **35** forms an H-bond with Val233 (Figure 3e), a similar interaction pattern to that seen for **36** (Figure 3f). Further elongation of the Boc-diaminoethane linker with three carbon atoms (**37**) reduced the SIRT2 inhibition activity (**36**: 77% vs **37**: 57%), indicating that a two-carbon spacer is preferred for the interaction with Val233. We also tested compound **38** with an alaninamide fragment, which is expected to interact directly with Val233 (Figure 3g). As expected, **38** showed potent SIRT2-inhibitory activity (81% inhibition). Furthermore, we screened the glycinamide precursors **39** and **40** to evaluate the effect of the glycine derivatives without any H-bond donor. The SIRT2-inhibitory activity of methyl ester derivative **39** was maintained, but that of the acid derivative **40** was not. As in the case of the previously reported glycinamide derivatives,[75] the above-mentioned studies suggest that glycinamide **54**[75] (Figure 3h, Table 1) is an optimal fragment to mimic acetyl-lysine in the substrate binding site, but

the interaction with Val233 alone did not allow full binding stabilization when longer fragments were applied, and consequently only mild inhibition was obtained.

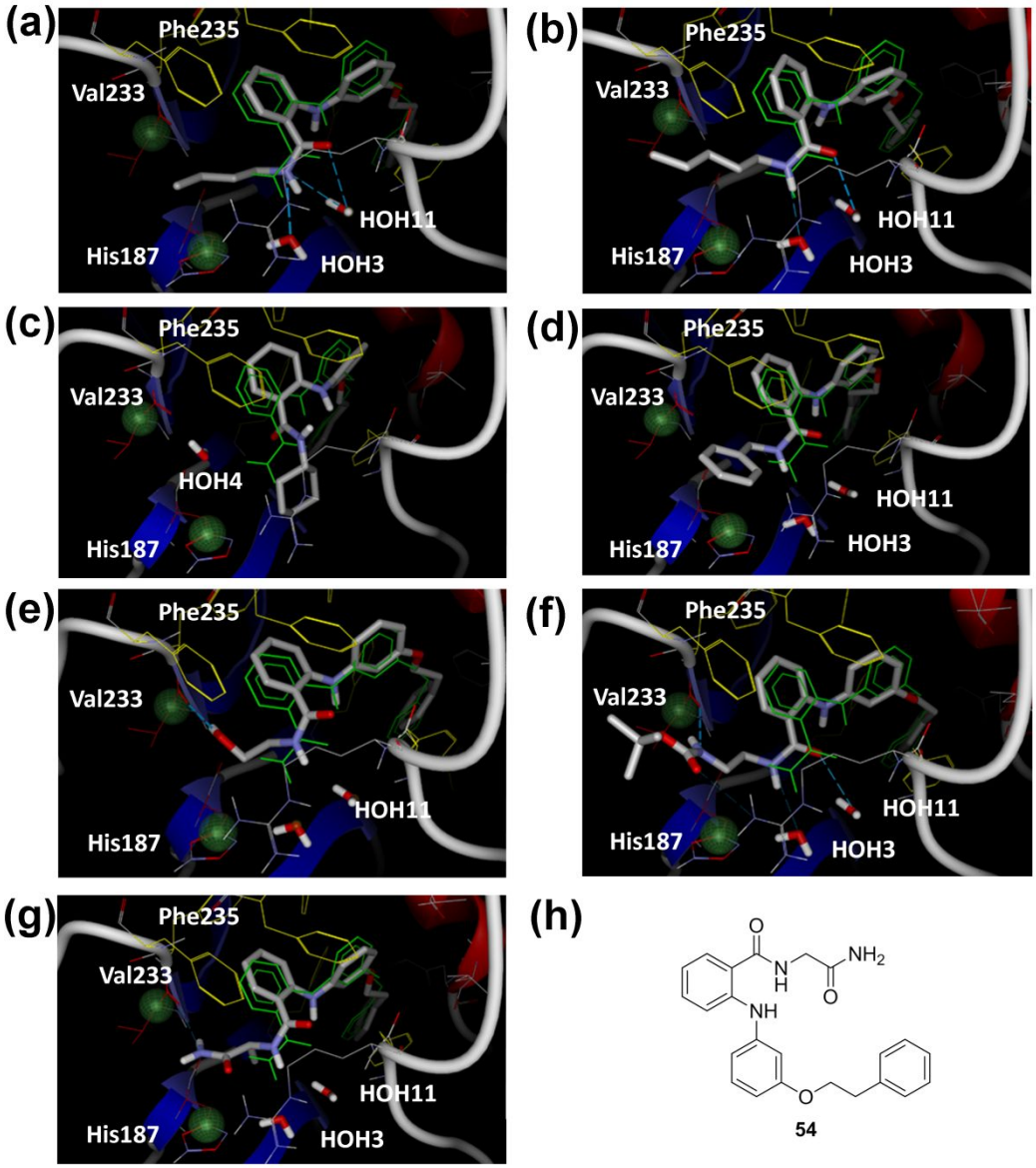

Figure 3. Docking poses of (a) **21**, (b) **23**, (c) **24**, (d) **26**, (e) **35**, (f) **36**, and (g) **38** in the SIRT2/NCO-90 crystal structure. Crystallized ligand NCO-90 and docking poses are colored in green and gray, respectively. His187 and Val233 are colored in red and delimited by green spheres. The phenylalanines composing the "selectivity pocket" are colored in yellow. H-bonds are represented by dashed lines. (h) Structure of glycinamide **54**.

A possible strategy to obtain potent SIRT2 inhibitors is the application of pseudopeptidic extensions in a similar manner to previously reported KPM-1, targeting Gly236, Glu237, and Gln267 of SIRT2 as potential H-bond sources (Figures 1e,f and 4). However, lysine derivatives with N-, C-terminal extensions have unfavorably high molecular weight or low stability/membrane permeability, with a nonoptimal drug-like profile. To overcome this dilemma, we designed compounds **41**–**43** (Scheme 3), in which NCO-90 is functionalized with a glycinamide linked with an alkyl chain spacer and terminal Boc or diketopiperazine moieties carrying H-bond acceptor/donor groups. Compounds **41** and **42** exhibited over 80% inhibition of SIRT2 at 10 μM, and **43** bearing diketopiperazine, a useful fragment to target key substrate amino acid residues, showed 92% inhibition. These results support the hypothesis that the diketopiperazine structure might establish H-bonds with Val233, Gly236, Glu237, and Gln267 of SIRT2. Furthermore, we designed and synthesized **53** as a thioamide analogue of **43** (Scheme 4 and Figure 4). We expected that the sulfur of **53** would nucleophilically attack NAD^+ at the active site of SIRT2 to enable stable conjugation with ADP-ribose (Supporting Information, Figure S1c), leading to potent SIRT2 inhibition in a similar manner to KPM-2 (Supporting Information, Figure S1b). As we expected, **53** potently inhibited SIRT2 even at 1 μM, with relatively low inhibitory activity toward SIRT1. Indeed, **53** was a more potent SIRT2 inhibitor than **8** and **43** at 1 μM (**53**: 73%; **8**: 47 %; **43**: 59%) (Table 1).

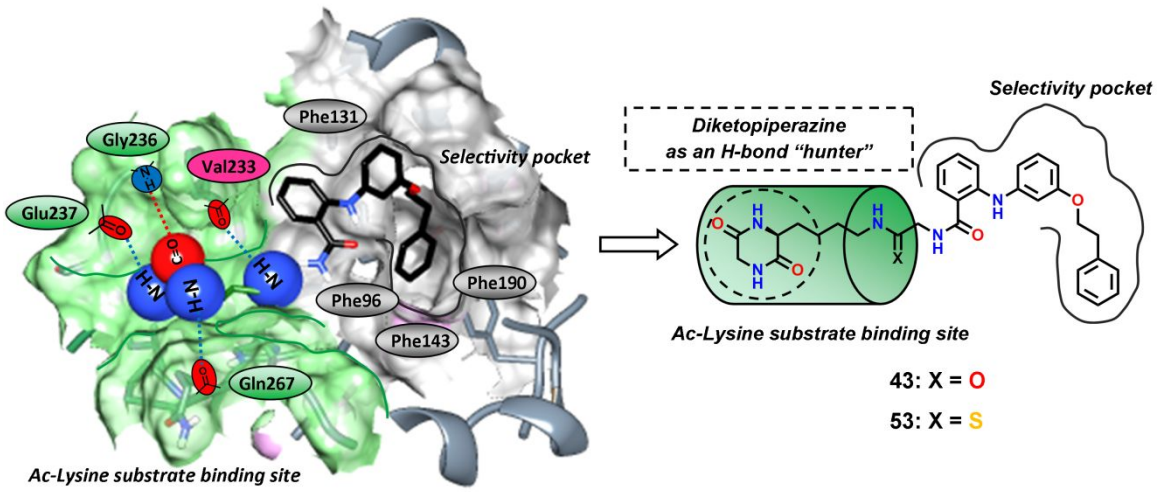

Figure 4. Rational design applied to NCO-90 targeting Val233, Gly236, Glu237, and Gln267 of SIRT2, which are involved in substrate binding stabilization. Conformation of NCO-90 bound to SIRT2 (PDB code: 5Y5N) is shown with key H-bonds indicated by dashed lines, together with the chemical structures of **43** and **53**.

Determination of IC_{50} values and evaluation of SIRT2-selectivity of selected inhibitors. Compounds **8**, **43**, and **53** were selected for further studies. First, the IC_{50} values for SIRT2 inhibition were determined (Table 2 and Figure 5). To assess the SIRT2-selectivity, we also evaluated SIRT1-, SIRT3-, and SIRT5-inhibitory activity (Table 2). Compound **8** strongly inhibited SIRT2 with an IC_{50} of 1.18 μM (Table 2 and Figure 5), which is in the same range as NCO-90. Notably, diketopiperazine derivative **43** and its thioamide analog **53** were potent and selective SIRT2 inhibitors (Table 2 and Figure 5). The SIRT2-inhibitory activity of **53** was greater than that of **43** (**43**: IC_{50} = 0.62 μM, **53**: IC_{50} = 0.31 μM), 6 times more potent than NCO-90, and similar to that of KPM-1 and SirReal2. In addition, **43** and **53** did not strongly inhibit SIRT1, SIRT3, or SIRT5: indeed, the SIRT2-inhibitory activity of **53** was over 220 times higher than the activities towards SIRT1 and SIRT3 (SIRT1 IC_{50}/SIRT2 IC_{50} = 250; SIRT3 IC_{50}/SIRT2 IC_{50} = 223). Accordingly, **43** and **53** are highly potent and selective SIRT2-inhibitors.

Table 2. IC_{50} values for compounds **8**, **43**, and **53**.

Cmpd.	IC_{50} ± SD [μM][a] or % inhibition[b]			
	SIRT1	SIRT2	SIRT3	SIRT5
NCO-90	17% at 100 μM	1.74 ± 0.26[c]	17% at 100 μM	8% at 100 μM
KPM-1	51% at 100 μM[d]	0.37 ± 0.03 [c]	61% at 100 μM[d]	6% at 100 μM[d]
SirReal2	-	0.30 ± 0.06 [c]	-	-
8	28% at 100 μM	1.18 ± 0.02	80% at 100 μM 63% at 50 μM	16% at 100 μM
43	13% at 100 μM	0.60 ± 0.10	17% at 100 μM	2% at 100 μM
53	77.4 ± 9.5	0.31 ± 0.12	69.2 ± 2.6	0% at 100 μM

[a]Fluor de Lys assay, values are calculated from three independent determinations giving altogether at least 21 data points. [b] Values represent the mean ± standard deviation of at least two experiments. [c] Data from ref 75. [d] Not fully soluble at tested concentration.

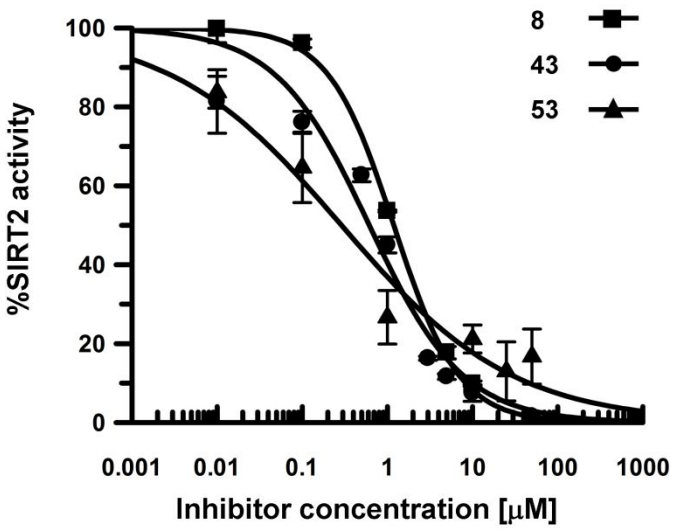

Figure 5. IC_{50} curves for inhibition of SIRT2 by compounds **8**, **43**, and **53**.

We also confirmed that compound **53** is not a pan assay interference compound (PAIN) using other enzymes and assay systems. The inhibitory activities of **53** against histone deacetylase 1 (HDAC1) and lysine demethylase 5A (KDM5A) were evaluated in fluorescence assay and AlphaScreen assay, respectively.[82,83] As a result, we found that **53** did

not inhibit HDAC1 and KDM5A at 2.5–100 μM (Supporting Information, Figure S2) and concluded that **53** is not a PAIN.

Inhibitory mechanism. We next investigated whether the inhibitory activity of **43** and **53** is competitive with respect to an acetylated lysine SIRT2 substrate. The Michaelis–Menten plot (Figure 6a,c) showed an increase of the apparent K_m with increasing **43** and **53** concentration at saturating NAD^+ concentration, and the K_i values were 0.47 ± 0.032 μM and 0.068 ± 0.0034 μM, respectively. A double-reciprocal plot of 1/V versus 1/[S] showed a series of regression lines that intersect on the 1/V axis, which is characteristic of competitive inhibition (Figure 6b,d).

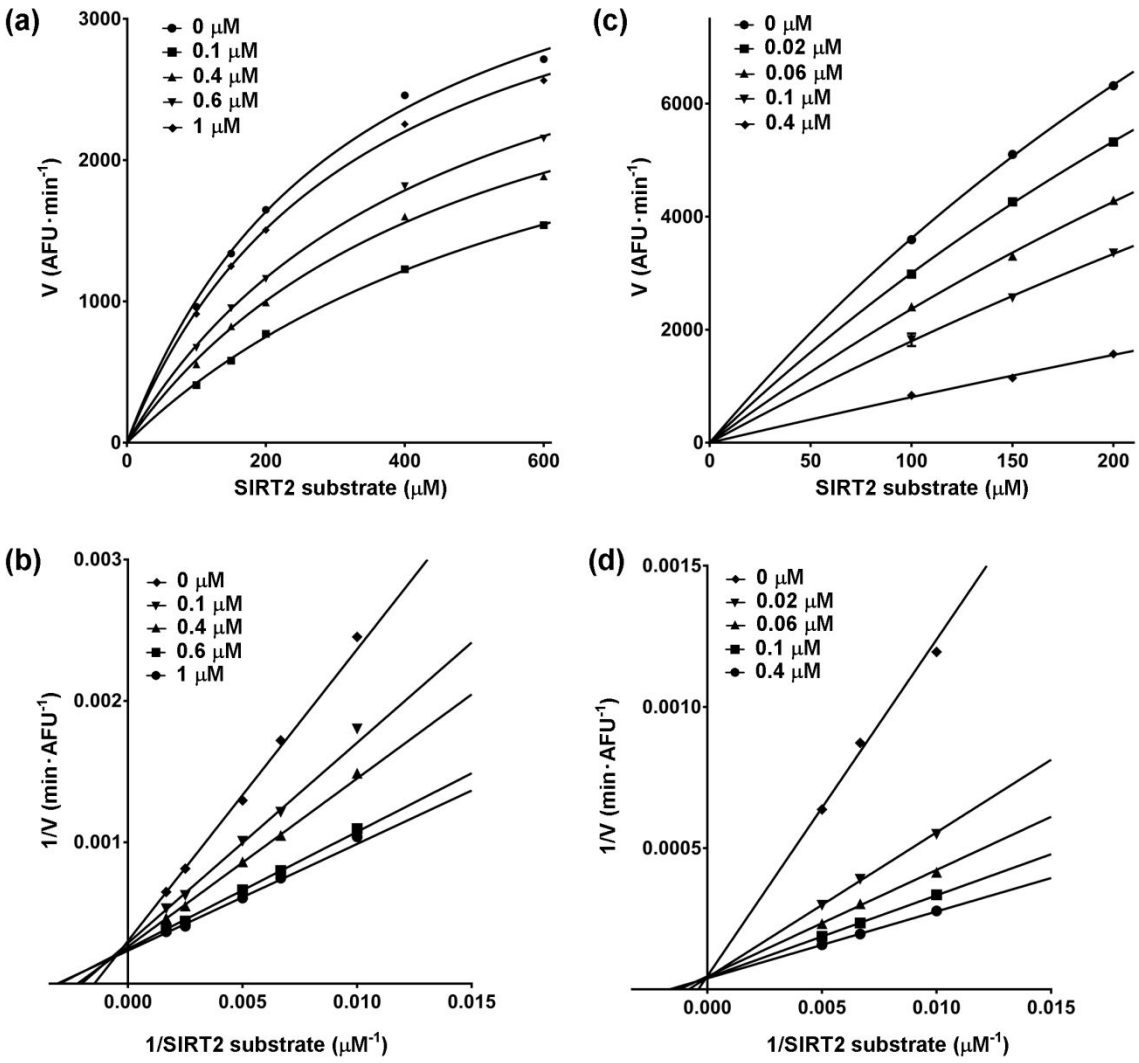

Figure 6. Competition analysis of compounds **43** and **53** with acetylated lysine substrate. (a) Michaelis-Menten plot showing acetylated Fluor de Lys SIRT2 substrate (μM) competition analysis at 0, 0.1, 0.4, 0.6, and 1 μM **43**. (b) Lineweaver-Burk plot 1/V versus reciprocal SIRT2 substrate concentration in the presence of 0, 0.1, 0.4, 0.6, and 1 μM **43**. (c) Michaelis-Menten plot showing Fluor de Lys SIRT2 substrate (μM) competition analysis at 0, 0.02, 0.06, 0.1, and 0.4 μM **53**. (d) Lineweaver-Burk plot 1/V versus reciprocal SIRT2 substrate concentration in the presence of 0, 0.02, 0.06, 0.1, and 0.4 μM **53**.

Next, we performed mass spectrometric analysis of an incubation mixture of SIRT2 with **53** to examine whether it inhibits SIRT2 by reacting with NAD^+ to afford **53**-ADP-ribose conjugate (Supporting Information, Figure S1). As depicted in Figure 7a, a significant peak was observed at *m/z* 1113.3. The peak corresponds to the predicted molecular weight of the **53**-ADP-ribose conjugate (Figure 7e). As this peak was not detected in the absence of SIRT2, NAD^+, or **53** (Figure 7b,c,d), these results suggest that the **53**-ADP-ribose conjugate was

generated as a result of SIRT2-catalyzed reaction of **53** with NAD^+, and **53** inactivates SIRT2 through mechanism-based inhibition.

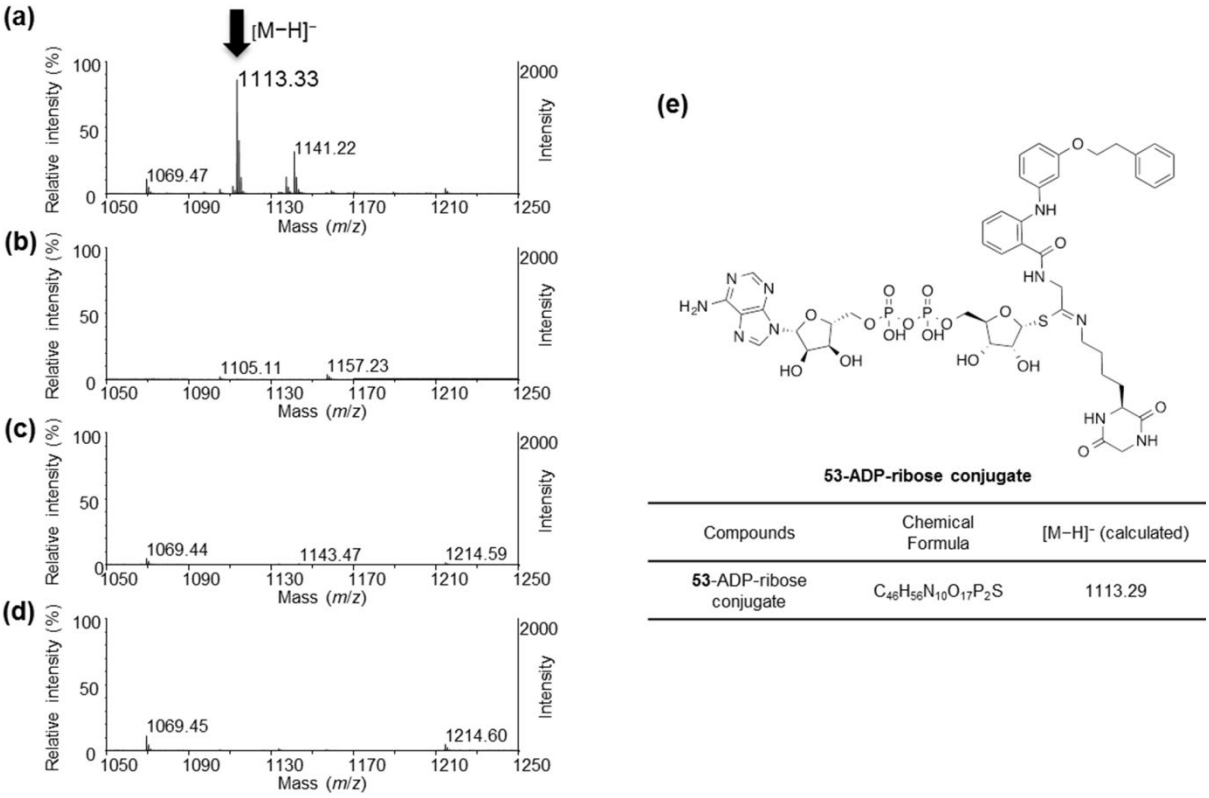

Compounds	Chemical Formula	[M−H]⁻ (calculated)
53-ADP-ribose conjugate	$C_{46}H_{56}N_{10}O_{17}P_2S$	1113.29

Figure 7. MALDI-TOF mass spectrometric detection of the ADP-ribose conjugate formed between **53** and NAD^+ (a) in the presence of SIRT2 and in the absence of (b) SIRT2, (c) NAD^+, or (d) compound **53**. (e) Chemical structure of the conjugate and the calculated *m*/*z* value for the $[M-H]^-$ ion.

Because compound **53** was a mechanism-based inhibitor, compound **43** was assumed to be hydrolyzed in a similar mechanism (Supporting Information, Figure S3a). Therefore, we also tested if hydrolysis of **43** occurs. We analyzed a mixture of SIRT2, NAD^+ and **43** by MS analysis. However, peaks which correspond to hydrolysis products were not detected (Supporting Information, Figure S3b–g), suggesting that **43** is not hydrolyzed by SIRT2. It indicates that **43** inhibits SIRT2 by occupying both SIRT2-selectivety pocket and substrate-binding site.

Cellular Assay. It has been reported that SIRT2 inhibition leads to growth inhibition of breast cancer cells.[73,75] Therefore, we investigated the antiproliferative activity of **43** and **53** towards breast cancer MCF-7 cells. NCO-90 was used as a reference compound. As shown in Figure 8a, **53** significantly reduced the proliferation of MCF-7 cells at 30 μM, and its antiproliferative activity was greater than that of **43** or NCO-90 at 30 μM (**53**: 96% cell growth inhibition; **43**: 40% cell growth inhibition; NCO-90: 30% cell growth inhibition). Moreover, we determined the half-maximal growth-inhibitory concentration (GI_{50}) of **53**. Compound **53** dose-dependently inhibited cell growth, and the GI_{50} value was 11.5 μM. We also compared the growth inhibitory activity of **53** with those of TM and KPM-2. As shown in Figure 8b, the growth inhibitory activity of **53** is superior to TM and comparable to KPM-2 (reported KPM-2 GI_{50}: 8.43 μM[75]). These results suggest that **53** with its diketopiperazine structure could be a good lead structure for the development of anticancer agents. We next examined the cellular SIRT2-selectivity of **53** by means of western blotting. As shown in Figure 9 and Supporting Information Figure S4, treatment of MCF-7 cells with 1–5 μM **53** induced the accumulation of acetylated α-tubulin, which is known to be a substrate of SIRT2.[84] On the other hand, **53** did not affect the level of acetylated lysine 9 in histone H3 (H3K9Ac), which is a SIRT1 substrate,[85–87] in MCF-7 cells. These results suggest that **53** selectively inhibits SIRT2 over SIRT1 *in cellulo*.

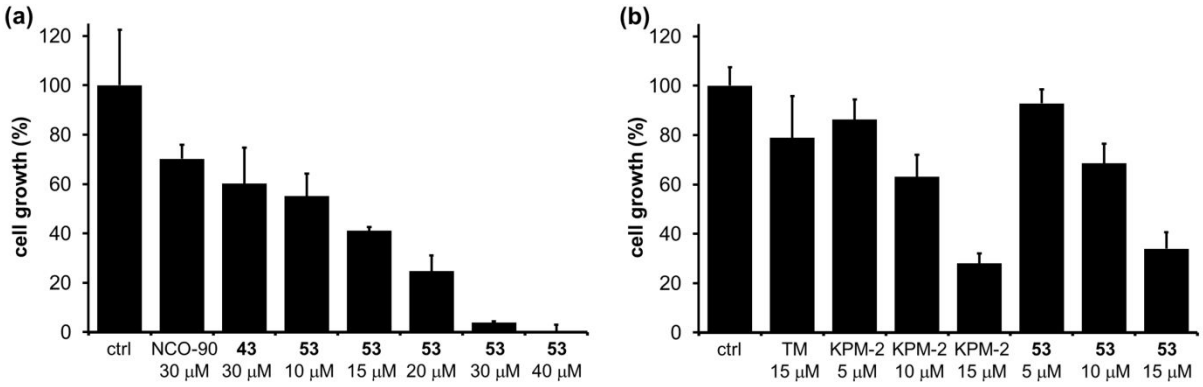

Figure 8. (a) Antiproliferative activity of NCO-90, **43**, and **53** towards MCF-7 cells. (b) Antiproliferative activity of TM, KPM-2, and **53** towards MCF-7 cells. Cells were exposed to test compound for 72 h. Values were calculated from three independent determinations.

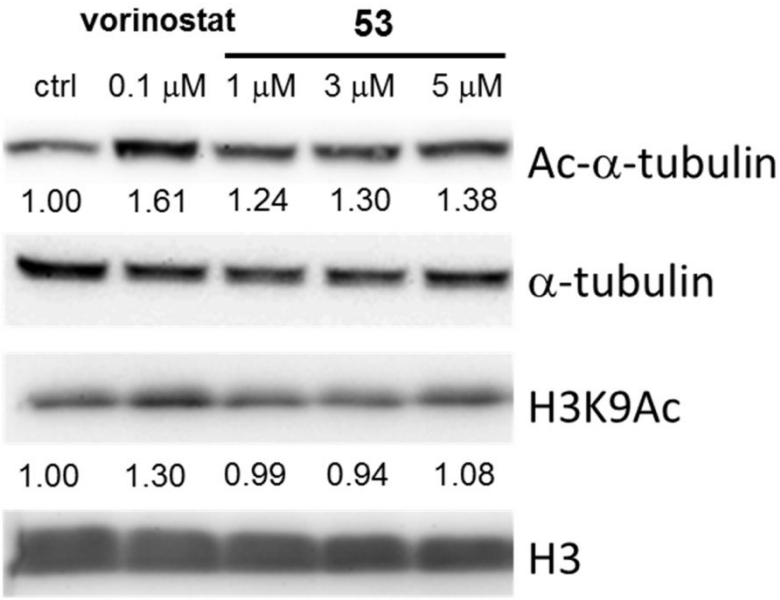

Figure 9. Western blot detection of acetylated α-tubulin or H3K9 in MCF-7 cells after 24 h treatment with **53** or vorinostat, which is a pan-HDAC inhibitor. The latter was used as a positive control that induces acetylation of both α-tubulin and H3K9. Values of Ac-α-tubulin and H3K9Ac ratio determined by optical density measurement of the blots are shown.

As it was previously suggested that SIRT2 inhibitors might be beneficial in the context of neurological disorders,[31–36] we examined the effect of **43** and **53** on the neurite outgrowth of Neuro-2a (N2a) cells (Figure 10 and Supporting Information, Figures S5 and S6). The treatment of N2a cells with **43** (0.2 and 2 μM) for 24 or 48 h did not significantly induce neurite outgrowth. On the other hand, treatment with **53** (2 μM) induced neurite outgrowth

and significantly increased the percentage of differentiated cells relative to the control group (**53** *vs.* ctrl for 24 h: 4.54 ± 0.48% *vs*. 2.53 ± 0.76%, $p < 0.0001$; for 48 h: 12.27 ± 1.28% *vs*. 4.18 ± 1.67%, $p < 0.001$). The percentages of differentiated cells were higher than those of NCO-90, TM, and KPM-2, which were used as a reference compound. As TM has a long fatty acyl chain, its plasma proteins binding rate is estimated to be high. Therefore, TM may easily bind to plasma proteins in medium and may not effectively inhibit SIRT2 in cells. These data suggest that **53** bearing a diketopiperazine structure may be a promising candidate or lead compound for therapeutic agents for neurological disorders.

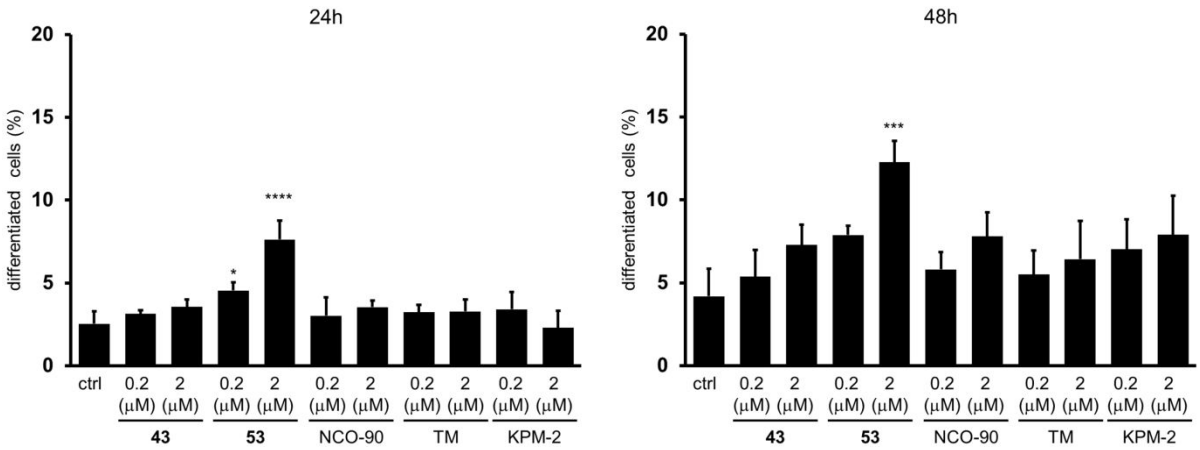

Figure 10. Effect of **43**, **53**, NCO-90, TM, and KPM-2 on N2a differentiation after 24 h or 48 h treatment, represented as the % of differentiated cells relative to the total counted cells (at least 100 cells for each condition). Bars represent the mean values ± SD from three independent experiments; *$p < 0.05$, ***$p < 0.001$, ****$p < 0.0001$, compared to the control group. For representative images showing N2a cells treated with **43**, **53**, NCO-90, TM, and KPM-2, see Supporting Information Figures S5 and S6.

CONCLUSION

To identify novel SIRT2-selective inhibitors, we used structure-based drug design based on the previously reported X-ray structure of SIRT2/NCO-90 complex. Using a simple fragment replacement strategy between NCO-90 and SirRea1, we found that 2-anilinobenzamide also

offers a versatile scaffold to probe the substrate-binding site and selectivity pocket. Furthermore, focusing on the key roles of Val233, Gly236, Glu237, and Gln267 in SIRT2 in stabilizing the binding of Ac-lysine-mimetic fragments, we developed a novel diketopiperazine structure as an "H-bond hunter" to target these amino acid residues. Compounds **43** and **53** with a diketopiperazine structure on a 2-anilinoamide scaffold were potent and selective SIRT2 inhibitors with inhibition profiles comparable to that of KPM-1. This finding opens up new perspectives in the design of previously unexplored drug-like sirtuin mechanism-based inhibitors. In cell-based assays, **53** showed potent antiproliferative activity in breast cancer cells and neurite outgrowth-inducing activity in N2a cells, suggesting that diketopiperazine/2-anilinobenzamide-based SIRT2 inhibitors are promising candidates or lead compounds for novel therapeutic agents for cancer and neurological disorders.

EXPERIMENTAL SECTION

Chemistry. The chemical reagents and solvents used in this study were commercial products of the highest available purity. Reagents and solvents were purchased from Sigma Aldrich, Wako Pure Chemical Industries, and TCI Tokyo Chemical Industry Co., Ltd. Organic solvents were dried over anhydrous sodium sulfate. Compounds **1**, **18**, **39**, and **40** were prepared according to Suzuki *et al.*[61] or Mellini *et al.*[75] (additional data given below). Commercially available compounds **4**, **5**, **9**, and **13** were used without purification. The synthetic route to **17** was adapted from Kaur *et al*.[88] NMR spectra were recorded on a Bruker Avance 300 AV (Bruker Biospin, Swizerland) spectrometer operating at 300.1 MHz (^{1}H) or 75.5 MHz (^{13}C). The chemical shift values are reported as δ (ppm) relative to TMS (tetramethylsilane) as an internal reference (δ = 0), and coupling constants are given in Hz. Positive/negative LRMS ion mass spectra were recorded on a Bruker HCT-Plus. The purity of all tested compounds was > 95%, except for **32** (92%), as determined by HPLC using a

Shimadzu UFLC (SPD-M20A UV detector, DGU-20A3R degassing unit, LC-20AD solvent delivery unit and CBM-20A system) and a C18 column (Inert Sustain, 4.6*150, 5 μM), at a flow rate of 1 mL/min, with UV detection (λ = 220 or 254 nm). HPLC conditions: eluent A: H_2O containing 0.1% TFA; eluent B: acetonitrile containing 0.1% TFA. Gradient: B: 0 to 20 min, 10–90%; 20 to 30 min, 90%; 30 to 40 min, 90–10%. Melting points were determined using a Yanaco Micro Melting Point apparatus. High-resolution mass spectra (HRMS) were recorded on a JEOL JMS-SX102A mass spectrometer or a Shimadzu LCMS-IT-TOF mass spectrometer.

Synthesis of 2-({3-[2-(naphthalen-2-yl)ethoxy]phenyl}amino)benzamide (2). To a solution of **1**[61] (0.22 g, 0.96 mmol) in dry acetone (15.0 mL) were added K_2CO_3 (0.40 g, 2.9 mmol) and 2-(2-bromoethyl)naphthalene[76] (0.45 g, 1.9 mmol). The mixture was heated at reflux under an N_2 atmosphere for 18 h, then insoluble materials were filtered off, and the filtrate was concentrated in vacuo. The crude product was purified by column chromatography on silica Kieselgel 60 (*n*-hexane:EtOAc = 6:4) to give a white solid (0.063 g, 0.16 mmol, 17%); R*f* = 0.28 (*n*-hexane:EtOAc = 6:4); m.p. 152–153 ºC; ^{1}H NMR (DMSO-d_6): δ 9.94 (s, 1H), 8.03 (s br, 1H), 7.89–7.82 (m overlap, 4H), 7.70–7.67 (m, 1H), 7.52–7.42 (m, 4H), 7.31–7.29 (m overlap, 2H), 7.20 (t, 1H, *J* = 8.3 Hz), 6.82–6.76 (m, 1H), 6.76–6.70 (m overlap, 2H), 6.58–6.54 (m, 1H), 4.27 (t, 2H, *J* = 6.8 Hz), 3.19 (t, 2H, *J* = 6.8 Hz); ^{13}C NMR (DMSO-d_6): δ = 171.17, 159.45, 144.62, 142.83, 136.04, 133.06, 131.99, 131.74, 130.09, 129.26, 127.64 (2C), 127.58, 127.40, 127.28, 126.99, 125.94, 125.33, 117.91, 115.30, 111.85, 108.06, 105.58, 67.92, 35.03; ESI-MS (*m*/*z*): 383.2 $[M + H]^+$; HRMS (EI) calcd for $C_{25}H_{22}N_2O_2$, 382.16813, found, 382.16749; HPLC: purity 98% at 254 nm, t_R: 21.9 min.

Synthesis of 3-[(2-carbamoylphenyl)amino]phenyl 2-[(4,6-dimethylpyrimidin-2-yl)thio]acetate (3). To a solution of 2-[(4,6-dimethylpyrimidin-2-yl)thio]acetic acid[76] (0.18 g, 0.91 mmol) in dry DMF, COMU® (0.47 g, 1.1 mmol) were added Et_3N (0.38 mL, 2.7

mmol) and **1** (0.21 g, 0.91 mmol) with cooling in an ice bath. The mixture was allowed to warm to room temperature. After 18 h, the resulting dark solution was diluted with brine (~30 mL) and extracted with EtOAc (4 x 40 mL). The combined organic phase was washed with saturated aqueous $NaHCO_3$ solution (twice) and brine, and dried over Na_2SO_4. Filtration, evaporation, and purification of the residue by column chromatography on silica Kieselgel 60 (*n*-hexane:EtOAc = 1:1) gave a light pink solid (0.098 g, 0.24 mmol, 27%); R*f* = 0.22 (*n*-hexane:EtOAc = 1:1); m.p. 71–72 ºC; ^{1}H NMR (DMSO-d_6): δ = 10.04 (s, 1H), 8.06 (s br, 1H), 7.71 (dd, 1H, *J* = 7.9, 1.1 Hz), 7.49 (s br, 1H), 7.33–7.25 (m overlap, 3H), 7.02–6.98 (m overlap, 2H), 6.87–6.82 (m overlap, 2H), 6.65 (dd, 1H, *J* = 7.9, 2.1 Hz), 4.18 (s, 2H), 2.32 (s, 6H); ^{13}C NMR (DMSO-d_6): δ = 171.02, 168.61, 167.91, 167.02, 151.45, 143.88, 142.97, 131.99, 130.23, 129.32, 118.63, 118.61, 116.44, 116.19, 115.57, 114.10, 111.43, 33.05, 23.25; ESI-MS (*m*/*z*): 409.1 $[M + H]^+$; HRMS (ESI) calcd for $C_{21}H_{20}N_4O_3SNa^+$, 431.1148; found, 431.1151; HPLC: purity 99% at 254 nm, t_R: 17.1 min.

Synthesis of 2-[(3-{2-[(4,6-dimethylpyrimidin-2-yl)thio]acetamido}phenyl)amino]benzamide (8). Step 1: preparation of 2-[(3-nitrophenyl)amino]benzamide (6). A solution of **4** (0.32 g, 2.4 mmol), **5** (0.4 g, 1.98 mmol), K_2CO_3 (0.38 g, 2.8 mmol), Pd_2dba_3 (0.16 g, 0.18 mmol) and XPhos (0.19 g, 0.39 mmol) in *tert*-BuOH (8 mL) was heated at reflux under an N_2 flow for 20 h, then EtOAc (~20 mL) was added to the reaction mixture. Insoluble materials were removed by filtration, and the filtrate was evaporated in vacuo. The residue was purified by column chromatography on silica Kieselgel 60 (*n*-hexane:EtOAc = 6:4) to give an orange solid (0.25 g, 0.99 mmol, 50%); R*f* = 0.29 (*n*-hexane:EtOAc = 6:4); ^{1}H NMR (DMSO-d_6): δ = 10.05 (s, 1H), 8.09 (s br, 1H), 7.91–7.90 (m, 1H), 7.76–7.69 (m overlap, 2H), 7.58–7.52 (m overlap, 3H), 7.43–7.39 (m overlap, 2H), 7.01–6.95 (m, 1H); ^{13}C NMR (DMSO-d_6): δ = 170.68, 148.71, 143.72, 142.49,

131.99, 130.54, 129.41, 124.31, 120.81, 120.13, 117.01, 115.02, 111.29; ESI-MS (*m*/*z*): 258.1 $[M + H]^+$.

Step 2: preparation of 2-[(3-aminophenyl)amino]benzamide (7). Pd/C 10% (0.036 g) was added to a suspension of **6** (0.15 g, 0.58 mmol) in MeOH (5 mL) and the mixture was stirred at room temperature under an H_2 atmosphere for 2 h. Pd/C was filtered off and the filtrate was evaporated in vacuo to provide a brown solid (0.13 g, 0.58 mmol, 100%); ^{1}H NMR (DMSO-d_6): δ = 9.86 (s, 1H), 8.00 (s br, 1H), 7.67 (d, 1H, *J* = 7.9 Hz), 7.43–7.24 (m overlap, 3H), 6.94 (t, 1H, *J* = 7.9 Hz), 6.75–7.70 (m, 1H), 6.39 (s, 1H), 6.31 (d, 1H, *J* = 7.7 Hz), 6.21 (d, 1H, *J* = 7.9 Hz), 5.04 (s, 2H); ^{13}C NMR (DMSO-d_6): δ = 171.45, 149.74, 145.54, 141.91, 132.01, 129.65, 129.25, 116.99, 116.82, 114.86, 108.44, 107.83, 105.39; ESI-MS (*m*/*z*): 228.1 $[M + H]^+$.

Step 3: 2-[(3-{2-[(4,6-dimethylpyrimidin-2-yl)thio]acetamido}phenyl)amino]benzamide (8). 2-[(4,6-Dimethylpyrimidin-2-yl)thio]acetic acid[77] (0.08 g, 0.40 mmol), EDCI·HCl (0.115 g, 0.60 mmol), anhydrous HOBt (0.081 g, 0.60 mmol), and Et_3N (0.167 mL, 1.2 mmol) were sequentially added to a solution of **7** (0.091 g, 0.4 mmol) in dry DMF (3 mL) with cooling in an ice bath. The mixture was stirred at room temperature for 17 h. The reaction was quenched by adding brine (~30 mL), and the whole was extracted with EtOAc (4 x 20 mL). The combined organic phase was washed with brine, and dried over Na_2SO_4. Filtration, evaporation in vacuo, and purification of the residue by column chromatography on silica Kieselgel 60 (*n*-hexane:EtOAc = 3:7) gave a light yellow solid (0.11 g, 0.28 mmol, 69%); R*f* = 0.32 (*n*-hexane:EtOAc = 3:7); m.p. 88–90 ºC; ^{1}H NMR (DMSO-d_6): δ = 10.19 (s, 1H), 10.04 (s, 1H), 8.05 (s br, 1H), 7.72 (d, 1H, *J* = 8.7 Hz), 7.52–7.42 (m overlap, 2H), 7.36–7.28 (m overlap, 2H), 7.23 (t, 1H, *J* = 7.9 Hz), 7.16–7.13 (m, 1H), 6.96 (s, 1H), 6.84–6.78 (m overlap, 2H), 4.02 (s, 2H), 2.34 (s, 6H); ^{13}C NMR (DMSO-d_6): δ = 171.29, 169.30, 166.93, 166.58, 144.70, 141.88, 139.98, 132.06,

129.66, 129.33, 117.90, 117.69, 116.02, 115.02, 114.59, 112.66, 109.89, 35.53, 23.29; ESI-MS (*m/z*): 408.1 $[M + H]^+$; HRMS (EI) calcd for $C_{21}H_{21}N_5O_2S$, 407.14160: found, 407.14248; HPLC: purity 99% at 254 nm, t_R: 14.9 min.

Synthesis of 2-{2-[(3-phenethoxyphenyl)amino]phenyl}acetamide (12). Step 1: preparation of 2-(2-nitrophenyl)acetamide (10). To a suspension of **9** (3.6 g, 20 mmol) in dry CH_2Cl_2 were added oxalyl chloride (3.5 mL, 40 mmol) and a catalytic amount of DMF with cooling on ice. After 10 min, the mixture was allowed to warm to room temperature and stirred for 3 h. The solvent was removed by evaporation in vacuo. The resulting acid chloride was dissolved in dry THF (6 mL) and the solution was added dropwise to a cooled flask containing NH_4OH 28% (50 mL). After 1 h, the precipitate was collected by filtration, and washed with H_2O (3 x 30 mL) and Et_2O (4 x 10 mL) to leave a light brown solid (2.37 g, 13 mmol, 65.8%). R*f* = 0.18 (*n*-hexane:EtOAc = 3:7); ^{1}H NMR (DMSO-d_6): δ = 8.00 (dd, 1H, *J* = 8.1, 1.3 Hz), 7.66 (dt, 1H, *J* = 7.6, 1.3 Hz), 7.54–7.43 (m overlap, 3H), 6.96 (s br, 1H), 3.85 (s, 2H); ^{13}C NMR (DMSO-d_6): δ = 170.46, 149.26, 133.41, 133.22, 131.06, 128.04, 124.35, 39.33; ESI-MS (*m/z*): 181.0 $[M + H]^+$.

Step 2: preparation of 2-(2-aminophenyl)acetamide (11). Compound **11** was prepared from **10** by using a similar procedure to that described for the preparation of **8** (Step 2); white solid (0.80 g, 5.3 mmol, 97%); R*f* = 0.25 (EtOAc); ^{1}H NMR (DMSO-d_6): δ = 7.48 (s br, 1H), 7.02–6.91 (m overlap, 3H), 6.65 (dd, 1H, *J* = 7.9, 1.1 Hz), 6.53 (td, 1H, *J* = 7.4, 1.1 Hz), 5.08 (s br, 2H), 3.26 (s, 2H); ^{13}C NMR (DMSO-d_6): δ = 173.03, 146.95, 130.29, 127.25, 120.55, 116.42, 115.05, 39.16; ESI-MS (*m/z*): 151.0 $[M + H]^+$.

Step 3: preparation of 2-{2-[(3-phenethoxyphenyl)amino]phenyl}acetamide (12). Compound **12** was prepared from **11** by using a similar procedure to that described for the preparation of **8** (Step 1); yellow sticky solid (0.28 g, 0.79 mmol, 68.7%); R*f* = 0.35 (*n*-hexane:EtOAc = 1:1); ^{1}H NMR (DMSO-d_6): δ = 8.21 (s, 1H), 7.62 (s br, 1H), 7.29–7.04 (m

overlap, 10H), 6.93–6.88 (m, 1H), 6.47–6.33 (m overlap, 3H), 4.10 (t, 2H, J = 6.8 Hz), 3.41 (s, 2H), 2.98 (t, 2H, J = 6.8 Hz); ^{13}C NMR (MeOH-d_4): δ = 177.19, 161.12, 147.04, 143.38, 139.61, 131.96, 130.91, 129.85, 129.25, 128.89, 128.50, 127.19, 123.21, 121.42, 110.41, 106.89, 104.05, 69.46, 40.11, 36.54. ESI-MS (*m*/*z*): 347.2 [M + H]$^+$; HRMS (EI) calcd for $C_{22}H_{22}N_2O_2$, 346.16813, found, 346.16806; HPLC: purity 96% at 254 nm, t_R: 19.5 min.

Synthesis of (*S*)-3-(4-Aminobutyl)piperazine-2,5-dione (17). Step 1: preparation of (*S*)-ethyl 2-(6-{[(benzyloxy)carbonyl]amino}-2-[(*tert*-butoxycarbonyl)amino]hexanamido)acetate (14). Compound **14** was prepared from **13** by using a similar procedure to that described for the preparation of compound **3**; light yellow oil (0.67 g, 1.4 mmol, 90%); R*f* = 0.71 (*n*-hexane:EtOAc = 2:8, visualized with phosphomolybdic acid); ^{1}H NMR ($CDCl_3$): δ = 7.36–7.30 (m overlap, 5H), 6.61 (s br, 1H), 5.17–5.05 (m overlap, 3H), 4.99–4.89 (m, 1H), 4.24–4.07 (m overlap, 3H), 4.03–3.99 (m, 2H), 3.22–3.16 (m, 2H), 1.92–1.80 (m, 1H), 1.58–1.38 (m, 13H), 1.25 (t, 3H, J = 7.2 Hz); ^{13}C NMR ($CDCl_3$): δ = 172.66, 169.82, 156.74, 155.85, 136.71, 128.54, 128.11, 80.14, 66.65, 61.54, 54.22, 50.65, 41.29, 40.48, 32.09, 29.43, 28.37, 22.42, 14.15; ESI-MS (*m*/*z*): 466.3 [M + H]$^+$.

Step 2: preparation of (*S*)-ethyl 2-(2-amino-6-{[(benzyloxy)carbonyl]amino}hexanamido)acetate trifluoroacetate (15). Trifluoroacetic acid (0.79 mL, 10.3 mmol) was slowly added to a cooled solution of **14** (0.60 g, 1.3 mmol) in dry CH_2Cl_2 (4 mL). The mixture was allowed to warm to room temperature and stirred overnight. Then, the solvent was removed under reduced pressure and the residue was washed with petroleum ether (twice) to afford **15** as a sticky solid (0.6 g, 1.3 mmol, 97%), which was used for the next step without purification; ^{1}H NMR (DMSO-d_6): δ = 8.86 (s br, 1H), 8.23–8.04 (m overlap, 3H), 7.42–7.28 (m, 5H), 7.26–7.13 (m, 1H), 5.01 (s, 2H), 4.14–3.80 (m overlap, 5H), 3.04–2.90 (m, 2H), 1.78–1.63 (m, 2H), 1.54–1.28 (m overlap, 4H),

1.22–1.15 (m, 3H); ^{13}C NMR ($CDCl_3$): δ = 169.81, 161.20, 160.68, 136.6, 128.73, 128.48, 128.00, 67.35, 62.23, 53.78, 41.54, 40.07, 30.68, 28.99, 21.18, 13.90; ESI-MS (*m/z*): 366.1 $[M + H]^+$.

Step 3: preparation of (*S*)-benzyl [4-(3,6-dioxopiperazin-2-yl)butyl]carbamate (16). To a solution of **15** (0.57 g, 1.19 mmol) in 1-butanol (8.4 mL) were added acetic acid (0.42 mL, 7.3 mmol) and *N*-methylmorpholine (0.84 mL, 7.6 mmol). The mixture was heated at reflux under an N_2 atmosphere for 220 min, and then cooled. The resulting white precipitate was collected by filtration and washed with 1-butanol (twice), H_2O (twice), and Et_2O (twice) to afford a white solid (0.26 g, 0.81 mmol, 68%); ^{1}H NMR (DMSO-d_6): δ = 8.15 (s, 1H), 7.98 (s, 1H), 7.47–7.23 (m overlap, 6H), 5.00 (s, 2H), 3.80–3.63 (m overlap, 3H), 3.07–2.92 (m, 2H), 1.77–1.57 (m, 2H), 1.48–1.20 (m, 4H); ^{13}C NMR (DMSO-d_6): δ = 168.01, 166.13, 156.09, 137.28, 128.35 (2C), 127.73, 65.14, 54.11, 44.30, 40.17 (under DMSO), 32.46, 29.12, 21.37; ESI-MS (*m/z*): 320.1 $[M + H]^+$.

Step 3: preparation of (*S*)-3-(4-aminobutyl)piperazine-2,5-dione (17). Compound **17** was prepared from **16** by using a similar procedure to that described for the preparation of **8** (Step 2); white solid (0.072 g, 0.39 mmol, 78%); ^{1}H NMR (5% D_2O in DMSO-d_6): δ = 3.86–3.66 (m overlap, 3H), 2.50–2.45 (m overlap, 2H), 1.67–1.58 (m, 2H), 1.38–1.18 (m overlap, 4H); ^{13}C NMR (DMSO-d_6): δ = 168.07, 166.12, 54.24, 44.29, 41.50, 33.07, 32.77, 21.47; ESI-MS (*m/z*): 186.2 $[M + H]^+$.

2-[(3-Phenethoxyphenyl)amino]benzoic acid (18);[75] m.p. 129–130 ºC; ^{1}H NMR (DMSO-d_6): δ = 13.05 (s br, 1H), 9.57 (s br, 1H), 7.88 (dd, 1H, *J* = 7.9, 1.7 Hz), 7.41–7.36 (m, 1H), 7.33–7.17 (m overlap, 7H), 6.81–6.75 (m overlap, 3H), 6.61 (dd, 1H, *J* = 7.6, 2.3 Hz), 4.17 (t, 2H, *J* = 6.8 Hz), 3.01 (t, 2H, *J* = 6.8 Hz); ^{13}C NMR (DMSO-d_6): δ = 169.88, 159.49, 146.73, 141.91, 138.38, 134.09, 131.85, 130.20, 128.93, 128.28, 126.24, 117.59, 114.31, 113.34, 112.96, 109.27, 107.23, 68.13, 34.95; ESI-MS (*m/z*): 331.9 $[M - H]^-$, 334.1 $[M + H]^+$; HRMS

(EI) calcd for $C_{21}H_{19}NO_3$, 333.13650, found, 333.13572; HPLC: purity 99% at 254 nm, t_R = 21.6 min.

Synthesis of 19–31. Compounds **19–31** were prepared from **18** and the corresponding amines by using a similar procedure to that described for the preparation of **8** (Step 3).

2-[(3-Phenethoxyphenyl)amino]-*N*-(prop-2-yn-1-yl)benzamide (19). Colorless sticky solid (0.028g, 0.077 mmol, 37%; R*f* = 0.26 (*n*-hexane:EtOAc = 8.5:1.5); ^{1}H NMR (DMSO-d_6): δ = 9.58 (s, 1H), 8.96 (t, 1H, *J* = 5.1 Hz), 7.62 (d, 1H, *J* = 8.7 Hz), 7.37–7.15 (m overlap, 8H), 6.86–6.80 (m, 1H), 6.73–6.68 (m overlap, 2H), 6.54 (dd, 1H, *J* = 7.7, 1.9 Hz), 4.17 (t, 2H, *J* = 6.8 Hz), 4.04–4.02 (m, 2H), 3.10 (t, 1H, *J* = 2.5 Hz), 3.01 (t, 2H, *J* = 6.8 Hz); ^{13}C NMR (CD_3OD): δ = 171.23, 161.31, 146.00, 144.49, 139.85, 133.24, 131.06, 130.00, 129.71, 129.39, 127.34, 120.33, 119.67, 117.25, 113.52, 109.48, 107.41, 80.84, 71.97, 69.81, 36.72, 29.68; ESI-MS (*m*/*z*): 371.1 $[M + H]^+$; HRMS (EI) calcd for $C_{24}H_{22}N_2O_2$, 370.16813, found, 370.16798; HPLC: purity 99% at 254 nm, t_R = 21.9 min.

2-[(3-Phenethoxyphenyl)amino]-*N*-propylbenzamide (20). Sticky solid; (0.059 g, 0.16 mmol, 66%); R*f* = 0.27 (*n*-hexane:EtOAc 8.5:1.5); ^{1}H NMR (DMSO-d_6): δ = 9.60 (s, 1H), 8.52 (t, 1H, *J* = 5.5 Hz), 7.63 (d, 1H, *J* = 8.3 Hz), 7.34–7.14 (m overlap, 8H), 6.87–6.81 (m, 1H), 6.71–6.66 (m overlap, 2H), 6.53 (dd, 1H, *J* = 7.6, 2.5 Hz), 4.17 (t, 2H, *J* = 6.8 Hz), 3.23–3.16 (m, 2H), 3.01 (t, 2H, *J* = 6.8 Hz), 1.58–1.46 (m, 2H), 0.88 (t, 3H, *J* = 7.4 Hz); ^{13}C-NMR (CD_3OD): δ = 171.57, 161.32, 145.38, 144.87, 139.84, 132.84, 131.05, 129.99, 129.63, 129.38, 127.33, 122.01, 120.05, 117.74, 113.04, 109.17, 106.92, 69.80, 42.46, 36.71, 23.64, 11.76. ESI-MS (*m*/*z*): 375.4 $[M + H]^+$; HRMS (EI) calcd for $C_{24}H_{26}N_2O_2$, 374.19943, found, 374.20034; HPLC: purity 99% at 254 nm, t_R: 23.3 min.

***N*-Butyl-2-((3-phenethoxyphenyl)amino)benzamide (21)**. Yellow sticky solid (0.056 g, 0.14 mmol, 69%); R*f* = 0.43 (*n*-hexane:EtOAc = 8:2); ^{1}H NMR (DMSO-d_6): δ = 9.59 (s, 1H), 8.50 (t, 1H, *J* = 5.7 Hz), 7.62 (d, 1H, *J* = 8.3 Hz), 7.36–7.14 (m overlap, 8H), 6.87–6.81

(m, 1H), 6.71–6.66 (m overlap, 2H), 6.52 (dd, 1H, J = 7.6, 1.7 Hz), 4.16 (t, 2H, 6.8 Hz), 3.27–3.20 (m, 2H), 3.03 (t, 2H, J = 6.8 Hz), 1.54–1.45 (m, 2H), 1.38–1.26 (m, 2H), 0.89 (t, 3H, J = 7.37 Hz). ^{13}C NMR (CD_3OD): δ = 171.47, 161.30, 145.30, 144.89, 139.82, 132.85, 131.05, 129.99, 129.65, 129.38, 127.33, 122.08, 120.12, 117.84, 112.95, 109.12, 106.82, 69.77, 40.45, 36.70, 32.55, 21.19, 14.13. ESI-MS (m/z): 389.2 [M + H]$^+$; HRMS (EI) calcd for $C_{25}H_{28}N_2O_2$, 388.21508; found, 388.21599; HPLC: purity 98% at 254 nm, t_R: 23.9 min.

***N*-Isopentyl-2-[(3-phenethoxyphenyl)amino]benzamide (22)**. Colorless sticky solid (0.028 g, 0.069 mmol, 63%); Rf = 0.26 (n-hexane:EtOAc = 9:1); ^{1}H NMR (DMSO-d_6): δ = 9.59 (s, 1H), 8.48 (t, 1H, J = 5.7 Hz), 7.60 (d, 1H, J = 7.9 Hz), 7.32–7.13 (m overlap, 8H), 6.86–6.82 (m, 1H), 6.70–6.66 (m overlap, 2H), 6.54 (dd, 1H, J = 7.9, 2.1 Hz), 4.16 (t, 2H, J = 6.8 Hz), 3.29–3.24 (m overlap H_2O, 2H), 3.0 (t, 2H, J = 6.9 Hz), 1.65–1.56 (m, 1H), 1.44–1.37 (m, 2H), 0.89 (d, 6H, J = 6.6 Hz). ^{13}C NMR (MeOH-d_4): δ = 171.44, 161.37, 145.22, 145.09, 139.89, 132.84, 131.06, 130.01, 129.70, 129.40, 127.35, 122.48, 120.29, 118.11, 112.89, 109.13, 106.77, 69.84, 39.34, 39.04, 36.74, 27.10, 22.85. ESI-MS (m/z): 403.3 [M + H]$^+$; HRMS (EI) calcd for $C_{26}H_{30}N_2O_2$, 402.23073, found, 402.23088; HPLC: purity 99% at 254 nm, t_R: 24.5 min.

***N*-Pentyl-2-[(3-phenethoxyphenyl)amino]benzamide (23)**. Colorless sticky solid (0.066 g, 0.16 mmol, 68%); Rf = 0.36 (n-hexane:EtOAc = 8.5:1.5); ^{1}H NMR (DMSO-d_6): δ = 9.58 (s, 1H), 8.50 (t, 1H, J = 5. 7 Hz), 7.62 (d, 1H, J = 7.6 Hz), 7.36–7.14 (m, overlap, 8H), 6.87–6.82 (m, 1H), 6.71–6.66 (m, overlap, 2H), 6.53 (dd, 1H, J = 7.4, 2.3 Hz), 4.16 (t, 2H, J = 6.8 Hz), 3.26–3.19 (m, 2H), 3.01 (t, 2H, J = 6.8 Hz), 1.55–1.46 (m, 2H), 1.33–1.24 (m overlap, 4H), 0.86 (t, 3H, J = 7.0 Hz); ^{13}C NMR (CD_3OD): δ = 171.46, 161.33, 145.25, 145.01, 139.85, 132.84, 131.05, 129.99, 129.67, 129.39, 127.34, 122.34, 120.23, 118.03, 112.92, 109.13, 106.80, 69.81, 40.72, 36.72, 30.31, 30.12, 23.42, 14.33; ESI-MS (m/z): 403.5 [M +

H]$^+$; HRMS (EI) calcd for $C_{26}H_{30}N_2O_2$, 402.23073, found, 402.23067; HPLC: purity 98% at 254 nm, t_R: 25.0 min.

***N*-Cyclohexyl-2-[(3-phenethoxyphenyl)amino]benzamide (24)**. White solid (0.082 g, 0.19 mmol, 82%); R*f* = 0.46 (*n*-hexane:EtOAc = 8:2); m.p. 134–136 ºC. ^{1}H-NMR (DMSO-d_6): δ = 9.50 (s, 1H), 8.28 (d, 1H, *J* = 7.9 Hz), 7.62 (d, 1H, *J* = 7.6 Hz), 7.35–7.13 (m overlap, 8H), 6.87–6.81 (m, 1H), 6.69–6.64 (m overlap, 2H), 6.52 (dd, 1H, *J* = 7.6, 1.7 Hz), 4.16 (t, 2H, *J* = 6.8 Hz), 3.79–3.69 (m, 1H), 3.01 (t, 2H, *J* = 6.8 Hz), 1.86–1.68 (m overlap, 4H), 1.64–1.55 (m, 1H), 1.36–1.21 (m overlap, 4H), 1.19–1.05 (m, 1H); ^{13}C NMR (DMSO-d_6): δ = 167.72, 159.44, 143.55, 143.12, 138.36, 131.50, 130.06, 128.96, 128.87, 128.22, 126.18, 120.14, 118.40, 115.81, 111.10, 107.64, 104.86, 67.99, 48.15, 34.90, 32.16, 25.18, 24.82; ESI-MS (*m*/*z*): 415.4 [M + H]$^+$; HRMS (EI) calcd for $C_{27}H_{30}N_2O_2$, 414.23073, found, 414.23051; HPLC: purity 98. % at 254 nm, t_R: 25.1 min.

2-[(3-Phenethoxyphenyl)amino]-*N*-phenylbenzamide (25). White solid (0.058 g, 0.14 mmol, 59%); R*f* = 0.34 (*n*-hexane: EtOAc = 8.5:1.5); m.p. 93–95 ºC; ^{1}H NMR (DMSO-d_6): δ = 10.32 (s br, 1H), 9.02 (s br, 1H), 7.76–7.69 (m overlap, 3H), 7.43–7.08 (m overlap, 11H), 6.98–6.92 (m, 1H), 6.74–6.69 (m overlap, 2H), 6.52 (dd, 1H, *J* = 8.1, 2.3 Hz), 4.16 (t, 2H, *J* = 6.8 Hz), 3.01 (t, 2H, *J* = 6.8 Hz); ^{13}C NMR (DMSO-d_6): δ = 167.45, 159.43, 143.54, 143.15, 138.81, 138.35, 131.98, 130.04, 129.37, 128.88, 128.51, 128.24, 126.19, 123.78, 121.12, 120.63, 118.86, 116.50, 111.23, 107.83, 105.07, 68.00, 34.90; ESI-MS (*m*/*z*): 409.3 [M + H]$^+$; HRMS (EI) calcd for $C_{27}H_{24}N_2O_2$, 408.18378, found, 408.18370; HPLC: purity 99% at 254 nm, t_R: 24.3 min.

***N*-Benzyl-2-[(3-phenethoxyphenyl)amino]benzamide (26)**. Colorless sticky solid (0.080 g, 0.19 mmol, 79%; R*f* = 0.30 (*n*-hexane:EtOAc = 8:2); ^{1}H NMR (DMSO-d_6): δ = 9.63 (s, 1H), 9.10 (t, 1H, *J* = 5.9 Hz), 7.72 (d, 1H, *J* =8.5 Hz), 7.38–7.15 (m overlap, 13H), 6.88–6.82 (m, 1H), 6.73–6.67 (m overlap, 2H), 6.53 (dd, 1H, *J* = 7.6, 1.7 Hz), 4.46 (d, 2H, *J* = 5.9 Hz),

4.17 (t, 2H, J = 6.8 Hz), 3.01 (t, 2H, J = 6.8 Hz); ^{13}C NMR (CD_3OD): δ = 171.44, 161.31, 145.59, 144.83, 140.07, 139.84, 133.04, 131.05, 129.99, 129.69, 129.51, 129.38, 128.43, 128.09, 127.33, 121.66, 120.11, 117.85, 113.12, 109.31, 107.03, 69.78, 44.25, 36.71; ESI-MS (m/z): 423.4 $[M + H]^+$; HRMS (EI) calcd for $C_{28}H_{26}N_2O_2$, 422.19943, found, 422.20007; HPLC: purity 99% at 254 nm, t_R: 24.0 min.

2-[(3-Phenethoxyphenyl)amino]-*N*-phenethylbenzamide (27). Yellow sticky solid (0.065 g, 0.15 mmol, 71%); Rf = 0.34 (n-hexane:EtOAc = 8:2); ^{1}H NMR (DMSO-d_6): δ = 9.53 (s, 1H), 8.61 (t, 1H, J = 5.48 Hz), 7.57 (d, 1H, J = 8.50 Hz), 7.35–7.15 (m overlap, 13H), 6.86–6.81 (m, 1H), 6.72–6.66 (m overlap, 2H), 6.53 (dd, 1H, J = 7.74, 1.70 Hz), 4.17 (t, 2H, J = 6.80 Hz), 3.50–3.42 (m, 2H), 3.02 (t, 2H, J = 6.80 Hz), 2.83 (t, 2H, J = 6.99 Hz); ^{13}C NMR (CD_3OD): δ = 171.53, 161.32, 145.30, 144.92, 140.54, 139.85, 132.86, 131.06, 130.00, 129.85, 129.61, 129.45, 129.40, 127.35, 127.30, 122.08, 120.09, 117.87, 113.04, 109.18, 106.94, 69.82, 42.28, 36.72, 36.50; ESI-MS (m/z): 437.2 $[M + H]^+$; HRMS (EI) calcd for $C_{29}H_{28}N_2O_2$, 436.21508; found, 436.21474; HPLC: purity 99% at 254 nm, t_R: 24.0 min.

***N*-(1-Benzylpiperidin-4-yl)-2-[(3-phenethoxyphenyl)amino]benzamide (28)**. White solid (0.068 g, 0.13 mmol, 64%); Rf = 0.31 (n-hexane:EtOAc:Et_3N = 6:4:0.0008); m.p. 49–51 ºC; ^{1}H-NMR (DMSO-d_6): δ = 9.46 (s, 1H), 8.32 (d, 1H, J = 7.7 Hz), 7.62 (d, 1H, J = 7.4 Hz), 7.36–7.13 (m overlap, 13H), 6.88–6.83 (m, 1H), 6.69–6.64 (m overlap, 2H), 6.52 (dd, 1H, J = 7.7, 1.9 Hz), 4.16 (t, 2H, J = 6.8 Hz), 3.79–3.69 (m, 1H), 3.45 (s, 2H), 3.01 (t, 2H, J = 6.8 Hz), 2.85–2.74 (m, 2H), 2.07–1.94 (m, 2H), 1.80–1.69 (m, 2H), 1.62–1.49 (m, 2H); ^{13}C-NMR (CD_3OD): δ = 170.72, 161.33, 145.20, 145.02, 139.82, 138.55, 132.96, 131.09, 130.69, 129.99, 129.39 (2C), 129.27 (2C), 128.37, 127.34, 122.74, 120.56, 118.53, 112.66, 109.04, 106.57, 69.78, 63.96, 53.34, 36.70, 32.21; ESI-MS (m/z): 506.3 $[M + H]^+$; HRMS (EI) calcd for $C_{33}H_{35}N_3O_2$, 505.27293, found, 505.27315; .HPLC: purity 99% at 254 nm, t_R: 18.5 min.

2-[(3-Phenethoxyphenyl)amino]-*N*-[(tetrahydro-2*H*-pyran-2-yl)oxy]benzamide (29). Light yellow solid (0.22 g, 0.5 mmol, 65%); R*f* = 0.22 (*n*-hexane:EtOAc = 8:2). m.p. 46–48 ºC. ^{1}H NMR (DMSO-d_6): δ = 11.64 (s br, 1H), 9.05 (s br, 1H), 7.52 (dd, 1H, *J* = 7.4, 1.1 Hz), 7.35–7.14 (m overlap, 8H), 6.87–6.71 (m, 1H), 6.73–6.68 (m, overlap, 2H), 6.54 (dd, 1H, *J* = 8.3, 1.7 Hz), 5.01 (pseudo s, 1H), 4.17 (t, 2H, *J* = 6.8 Hz), 4.07–3.99 (m, 1H), 3.55–3.49 (m, 1H), 3.02 (t, 2H, *J* = 6.80 Hz), 1.77–1.65 (m overlap, 3H), 1.61–1.48 (m overlap, 3H); ^{13}C NMR (CD_3OD): δ = 169.28, 161.26, 145.74, 144.35, 139.76, 133.40, 131.08, 129.97, 129.74, 129.37, 127.32, 119.76, 118.67, 117.36, 113.30, 109.45, 107.29, 103.46, 69.75, 63.22, 36.67, 29.05, 26.16, 19.49; ESI-MS (*m*/*z*): 433.2 [M + H]$^+$; HRMS (EI) calcd for $C_{26}H_{28}N_2O_4$, 432.20491, found, 432.20484; HPLC: purity 97% at 254 nm, t_R: 22.0 min.

***N*,*N*-Diethyl-2-[(3-phenethoxyphenyl)amino]benzamide (30)**. White solid (0.069 g, 0.17 mmol, 74%); R*f* = 0.23 (*n*-hexane:EtOAc = 8:2); m.p. 99–101 ºC; ^{1}H NMR (DMSO-d_6): δ = 7.37 (s, 1H), 7.31–7.17 (m overlap, 8H), 7.08–6.97 (m overlap, 2H), 6.57–6.55 (m overlap 2H), 6.39–6.36 (m, 1H), 4.11 (t, 2H, *J* = 6.8 Hz), 3.46–3.34 (m broad, 2H), 3.22–3.08 (m broad, 2H), 3.00 (t, 2H, *J* = 7.0 Hz), 1.10–0.87 (m broad, 6H); ^{13}C NMR (CD_3OD): δ = 172.27, 161.32, 146.15, 141.50, 139.88, 131.12, 130.97, 129.99, 129.38, 128.99, 128.67 (2C), 127.33, 122.43, 121.02 (2C), 111.31, 108.10, 105.16, 69.76, 36.71; ESI-MS (*m*/*z*): 389.4 [M + H]$^+$; HRMS (EI) calcd for $C_{25}H_{28}N_2O_2$, 388.21508, found, 388.21500; HPLC: purity 99% at 254 nm, t_R: 22.7 min.

Morpholino{2-[(3-phenethoxyphenyl)amino]phenyl}methanone (31). White solid (0.044 g, 0.11 mmol, 53%); R*f* = 0.49 (*n*-hexane:EtOAc = 6:4). m.p. 150–152 ºC; ^{1}H NMR (DMSO-d_6): δ = 7.69 (s, 1H), 7.35–7.19 (m overlap, 8H), 7.08 (t, 1H, *J* = 7.7 Hz), 7.02–6.97 (m, 1H), 6.60–6.57 (m overlap, 2H), 6.42–6.39 (m, 1H), 4.12 (t, 2H, *J* = 6.8 Hz), 3.58–3.39 (m broad, 8H), 3.0 (t, 2H, *J* = 6.8 Hz); ^{13}C NMR (DMSO-d_6): δ = 167.73, 159.26, 144.90, 139.80, 138.36, 130.01, 129.72, 128.87, 128.66, 128.22, 126.52, 126.18, 121.14, 119.62,

109.29, 106.28, 103.10, 67.90, 65.85, 34.90; ESI-MS (*m*/*z*): 403.2 [M + H]$^+$; HRMS (EI) calcd for $C_{25}H_{26}N_2O_3$, 402.19435, found, 402.19528; HPLC: purity 99% at 254 nm, t_R: 20.2 min.

Synthesis of *N*-hydroxy-2-[(3-phenethoxyphenyl)amino]benzamide (32). A solution of TsOH·H_2O (0.0044 g, 0.023 mmol) in MeOH (0.5 mL) was added to a solution of **29** (0.10 g, 0.23 mmol) in MeOH (5 mL). The mixture was stirred at room temperature for 3.5 h. The solvent was removed by evaporation, and the residue was purified by column chromatography on silica Kieselgel 60 (CH_2Cl_2: MeOH = 40:1) to furnish a brown sticky solid (0.029 g, 0.083 mmol, 37%); R*f* = 0.32 (CH_2Cl_2: MeOH = 20:1); ^{1}H NMR (DMSO-d_6): δ = 11.20 (s br, 1H), 9.17 (s br, 1H), 9.10 (s br, 1H), 7.46 (d, 1H, *J* = 7.7 Hz), 7.32–7.14 (m overlap, 8H), 6.85–6.80 (m, 1H), 6.70–6.67 (m overlap, 2H), 6.52 (dd, 1H, *J* = 8.1, 2.1 Hz), 4.16 (t, 2H, *J* = 6.8 Hz), 3.02 (t, 2H, *J* = 6.8 Hz); ^{13}C NMR (CD_3OD): δ = 169.61, 161.34, 145.68, 144.49, 139.87, 133.10, 131.09, 130.02, 129.41, 129.30, 127.37, 119.74, 118.93, 117.20, 113.30, 109.34, 107.20, 69.83, 36.73; ESI-MS (*m*/*z*): 349.2 [M + H]$^+$, 347.0 [M - H]$^-$; HRMS (EI) calcd for $C_{21}H_{20}N_2O_3$, 348.14740, found, 348.14827; HPLC: purity 92% at 254 nm, t_R: 18.7 min.

Synthesis of 33–39. Compounds **33–39** were prepared from **18** and the corresponding amines by using a similar procedure to that described for the preparation of **8** (Step 3).

***N*-Methoxy-2-[(3-phenethoxyphenyl)amino]benzamide (33)**. Light yellow solid (0.060 g, 0.16 mmol, 55%); R*f* = 0.29 (*n*-hexane:EtOAc = 7:3); m.p. 148–150 ºC; ^{1}H NMR (DMSO-d_6): δ = 11.68 (s br, 1H), 9.10 (s br, 1H), 7.47 (dd, 1H, *J* = 7.7, 1.3 Hz), 7.37–7.13 (m overlap, 8H), 6.85–6.80 (m, 1H), 6.71–6.66 (m overlap, 2H), 6.54–6.51 (m, 1H), 4.15 (t, 2H, *J* = 7.0 Hz), 3.67 (s, 3H), 3.00 (t, 2H, *J* = 7.0 Hz); ^{13}C NMR (DMSO-d_6): δ = 166.15, 159.42, 143.73, 142.88, 138.36, 132.07, 130.08, 128.90, 128.47, 128.25, 126.20, 118.16, 117.41, 116.04, 111.43, 107.96, 105.24, 68.00, 63.17, 34.90. ESI-MS (*m*/*z*): 363.2 [M + H]$^+$; HRMS

(EI) calcd for $C_{22}H_{22}N_2O_3$, 362.16305, found, 362.16288; HPLC: purity 96% at 254 nm, t_R: 20.4 min.

***N*-[2-(Dimethylamino)ethyl]-2-[(3-phenethoxyphenyl)amino]benzamide (34)**. Colorless sticky solid (0.055 g, 0.14 mmol, 65%); R*f* = 0.15 (EtOAc:MeOH:Et_3N = 9:1:0.0009); ^{1}H NMR (DMSO-d_6): δ = 9.52 (s, 1H), 8.41 (t, 1H, *J* = 5.7 Hz), 7.61 (d, 1H, *J* = 8.7 Hz), 7.36–7.14 (m overlap, 8H), 6.87–6.82 (m, 1H), 6.71–6.66 (m overlap, 2H), 6.53 (dd, 1H, *J* = 7.55, 1.70 Hz), 4.16 (t, 2H, *J* = 6.8 Hz), 3.35–3.29 (t under H_2O signal, 2H), 3.02 (t, 2H, *J* = 6.80 Hz), 2.37 (t, 2H, *J* = 6.8 Hz), 2.16 (s, 6H); ^{13}C NMR (CD_3OD): δ = 171.43, 161.29, 145.42, 144.84, 139.82, 132.99, 131.05, 129.99, 129.70, 129.38, 127.33, 121.64, 120.04, 117.79, 113.07, 109.15, 106.98, 69.75, 59.07, 45.48, 38.21, 36.70; ESI-MS (*m*/*z*): 404.2 $[M + H]^+$; HRMS (EI) calcd for $C_{25}H_{29}N_3O_2$, 403.22598, found, 403.22641; HPLC: purity 99% at 254 nm, t_R: 16.5 min.

***N*-(2-Hydroxyethyl)-2-[(3-phenethoxyphenyl)amino]benzamide (35)**. Light yellow solid; (0.082 g, 0.22 mmol, 73%; R*f* = 0.38 (*n*-hexane:EtOAc = 3:7; m.p. 107–109 ºC; ^{1}HNMR (DMSO-d_6): δ = 9.58 (s, 1H), 8.45 (t, 1H, *J* = 5.48 Hz), 7.64 (dd, 1H, *J* = 7.4, 0.9 Hz), 7.34–7.14 (m overlap, 8H), 6.86–6.80 (m, 1H), 6.71–6.65 (m overlap, 2H), 6.51 (dd, 1H, *J* = 7.7, 2.1 Hz), 4.70 (t, 1H, *J* = 5.5 Hz), 4.16 (t, 2H, *J* = 6.8 Hz), 3.53–3.47 (m, 2H), 3.34–3.28 (m under H_2O signal, 2H), 3.01 (t, 2H, *J* = 6.8 Hz); ^{13}C NMR (DMSO-d_6): δ = 168.70, 159.43, 143.79, 142.96, 138.35, 131.65, 130.07, 128.88, 128.80, 128.23, 126.18, 119.43, 118.26, 115.60, 111.38, 107.81, 105.13, 67.99, 59.56, 41.95, 34.90; ESI-MS (*m*/*z*): 377.3 $[M + H]^+$; HRMS (EI) calcd for $C_{23}H_{24}N_2O_3$, 376.17870, found, 376.17816; HPLC: purity 99% at 254 nm, t_R: 19.0 min.

***tert*-Butyl (2-{2-[(3-phenethoxyphenyl)amino]benzamido}ethyl)carbamate (36)**. White solid (0.069 g, 0.15 mmol, 70%); R*f* = 0.23 (*n*-hexane:EtOAc = 7:3); m.p. 59–61 ºC; ^{1}H NMR (DMSO-d_6): δ = 9.57 (s, 1H), 8.48 (t, 1H, *J* = 5.1 Hz), 7.63 (d, 1H, *J* = 7.9 Hz), 7.33–

7.14 (m overlap, 8H), 6.88–6.81 (m overlap, 2H), 6.72–6.66 (m overlap, 2H), 6.53 (dd, 1H, *J* = 7.7, 1.9 Hz), 4.16 (t, 2H, *J* = 6.8 Hz), 3.26–3.24 (m overlap, 2H), 3.12–3.08 (m, 2H), 3.01 (t, 2H, *J* = 6.8 Hz), 1.36 (s, 9H); ^{13}C NMR (CD_3OD): δ = 171.85, 161.30, 158.78, 145.59, 144.70, 139.83, 132.98, 131.04, 129.99, 129.73, 129.38, 127.34, 121.31, 119.80, 117.45, 113.21, 109.25, 107.11, 80.19, 69.80, 41.03, 40.90, 36.71, 28.72; ESI-MS (*m*/*z*): 476.3 [M + H]$^+$; HRMS (EI) calcd for $C_{28}H_{33}N_3O_4$, 475.24711, found, 475.24659; HPLC: purity 99% at 254 nm, t_R: 22.6 min.

***tert*-Butyl (3-{2-[(3-phenethoxyphenyl)amino]benzamido}propyl)carbamate (37)**. Colorless sticky solid (0.064 g, 0.13 mmol, 63%); R*f* = 0.27 (*n*-hexane:EtOAc = 7:3); ^{1}H NMR (DMSO-d_6): δ = 9.57 (s, 1H), 8.47 (t, 1H, *J* = 5.48 Hz), 7.61 (d, 1H, *J* = 7.55 Hz), 7.31–7.13 (m overlap, 8H), 6.86–6.78 (m overlap, 2H), 6.70–6.66 (m overlap, 2H), 6.54 (dd, 1H, *J* = 8.12, 2.08 Hz), 4.16 (t, 2H, *J* = 6.80 Hz), 3.26–3.19 (m, 2H), 3.04–2.93 (m overlap, 4H), 1.65–1.57 (m, 2H), 1.36 (s, 9H); ^{13}C NMR (MeOH-d_4): δ = 171.65, 161.33, 145.47, 144.87, 139.87, 132.94, 131.05, 130.00 (2C), 129.67, 129.40, 127.35, 121.82, 120.06, 117.77, 113.12, 109.22, 107.00, 80.06, 69.83, 38.81, 37.99, 36.73, 30.76, 28.77; ESI-MS (*m*/*z*): 490.3 [M + H]$^+$; HRMS (EI) calcd for $C_{29}H_{35}N_3O_4$, 489.26276: found, 489.26421; HPLC: purity 99% at 254 nm, t_R: 23.1 min.

(*S*)-*N*-(1-Amino-1-oxopropan-2-yl)-2-((3-phenethoxyphenyl)amino)benzamide (38). White solid (0.073 g, 0.18 mmol, 75%); R*f* = 0.42 (EtOAc:*n*-hexane = 8:2); m.p. 133–135 ºC; ^{1}H NMR (DMSO-d_6): δ = 9.40 (s, 1H), 8.47 (d, 1H, *J* = 7.36 Hz), 7.71 (d, 1H, *J* = 7.6 Hz), 7.41–7.14 (m overlap, 9H), 7.02 (s br, 1H), 6.88–6.83 (m, 1H), 6.72–6.66 (m overlap, 2H), 6.53 (dd, 1H, *J* = 6.4, 1.7 Hz), 4.42–4.32 (m, 1H), 4.16 (t, 2H, *J* = 6.8 Hz), 3.02 (t, 2H, *J* = 6.8 Hz), 1.31 (d, 3H, *J* = 7.4 Hz); ^{13}C NMR (DMSO-d_6): δ = 174.34, 168.20, 159.40, 143.54, 143.14, 138.36, 131.68, 130.03, 129.17, 128.87, 128.23, 126.18, 119.89, 118.44, 115.78, 111.38, 107.73, 105.14, 67.99, 48.60, 34.90, 17.80. ESI-MS (*m*/*z*): 404.4 [M + H]$^+$; HRMS

(EI) calcd for $C_{24}H_{25}N_3O_3$, 403.18960; found, 403.19001; HPLC: purity 99% at 254 nm, t_R: 19.0 min.

Methyl 2-{2-[(3-phenethoxyphenyl)amino]benzamido}acetate (39).[75] ^{1}H NMR (DMSO-d_6): δ = 9.57 (s, 1H), 8.99 (t, 1H, *J* = 5.5 Hz), 7.70 (d, 1H, *J* = 8.9 Hz), 7.39-7.16 (m overlap, 8H), 6.88–6.83 (m, 1H), 6.74–6.69 (m overlap, 2H), 6.56 (dd, 1H, *J* = 8.3, 1. 9 Hz), 4.17 (t, 2H, *J* = 6.8 Hz), 4.00 (d, 2H, *J* = 5.7 Hz), 3.65 (s, 3H), 3.02 (t, 2H, *J* = 6.8 Hz); ^{13}C NMR (CD_3OD): δ = 172.15, 171.94, 161.30, 145.98, 144.48, 139.85, 133.30, 131.04, 130.00, 129.74, 129.39, 127.35, 120.25, 119.65, 117.19, 113.54, 109.50, 107.47, 69.81, 52.66, 42.16, 36.71; ESI-MS (*m*/*z*): 405.1 $[M + H]^+$; HRMS (EI) calcd for $C_{24}H_{24}N_2O_4$, 404.17361; found, 404.17292; HPLC: purity 99% at 254 nm, t_R: 21.4 min.

2-{2-[(3-Phenethoxyphenyl)amino]benzamido}acetic acid (40).[75] ^{1}H NMR (DMSO-d_6): δ = 9.58 (s, 1H), 8.87 (t, 1H, *J* = 5.9 Hz), 7.68 (d, 1H, *J* = 7.6 Hz), 7.38–7.15 (m overlap, 8H), 6.88–6.82 (m, 1H), 6.74–6.69 (m overlap, 2H), 6.55 (dd, 1H, *J* = 8.3, 2.1 Hz), 4.17 (t, 2H, *J* = 6.8 Hz), 3.90 (d, 2H, *J* = 5.9 Hz), 3.01 (t, 2H, *J* = 6.8 Hz); ^{13}C NMR (CD_3OD): δ = 173.33, 171.88, 161.25, 145.84, 144.47, 139.82, 133.19, 131.01, 129.99, 129.73, 129.38, 127.33, 120.46, 119.64, 117.10, 113.50, 109.42, 107.40, 69.77, 42.07, 36.68; ESI-MS (*m*/*z*): 391.1 $[M + H]^+$, 389.0 $[M - H]^-$; HRMS (EI) calcd for $C_{23}H_{22}N_2O_4$, 390.15901, found, 390.15796; HPLC: purity 99% at 254 nm, t_R: 19.3 min.

Synthesis of compounds 41–43. Compounds **41–43** were prepared from **40** and the corresponding amines by using a similar procedure to that described for the preparation of compound **8** (step 3).

***tert*-Butyl [4-(2-{2-[(3-phenethoxyphenyl)amino]benzamido}acetamido)butyl]carbamate (41)**. White solid (0.065 g, 0.11 mmol, 65%); R*f* = 0.30 (*n*-hexane:EtOAc = 2:8); m.p. 58–60°C; ^{1}H NMR (DMSO-d_6): δ = 9.55 (s, 1H), 8.71 (t, 1H, *J* = 6.0 Hz), 7.90 (t, 1H, *J* = 5.5 Hz), 7.70 (d, 1H, *J*

= 7.6 Hz), 7.37–7.15 (m overlap, 8H), 6.88–6.82 (m, 1H), 6.77–6.68 (m overlap, 3H), 6.54 (dd, 1H, *J* = 8.1, 2.3 Hz), 4.17 (t, 2H, *J* = 6.8 Hz), 3.82 (d, 2H, *J* = 5.9 Hz), 3.06–3.00 (m overlap, 4H), 2.93–2.87 (m, 2H), 1.42–1.32 (m overlap, 13H); ^{13}C NMR (CD_3OD): δ = 171.84, 171.71, 161.26, 158.45, 145.79, 144.62, 139.80, 133.25, 131.05, 130.00, 129.85, 129.39, 127.35, 120.68, 119.83, 117.46, 113.27, 109.32, 107.20, 79.82, 69.76, 43.89, 40.92, 40.10, 36.69, 28.78, 28.23, 27.58; ESI-MS (*m/z*): 561.5 $[M + H]^+$; HRMS (EI) calcd for $C_{32}H_{40}N_4O_5$, 560.29986, found, 560.30094; HPLC: purity 99% at 254 nm, t_R: 21.4 min.

***tert*-Butyl [5-(2-{2-[(3-phenethoxyphenyl)amino]benzamido}acetamido)pentyl]carbamate (42)**. White solid; (0.071 g, 0.12 mmol, 69%); R*f* = 0.42 (*n*-hexane:EtOAc = 2:8); m.p. 55–57°C; ^{1}H NMR (DMSO-d_6): δ = 9.54 (s, 1H), 8.70 (t, 1H, *J* = 5.9 Hz), 7.89 (t, 1H, *J* = 5.9 Hz), 7.68 (d, 1H, *J* = 7.6 Hz), 7.37–7.15 (m overlap, 8H), 6.87–6.82 (m ,1H), 6.74–6.68 (m overlap, 3H), 6.54 (dd, 1H, *J* = 7.7, 1.9 Hz), 4.17 (t, 2H, *J* = 6.8 Hz), 3.81 (d, 2H, *J* = 5.9 Hz), 3.08–3.00 (m overlap, 4H), 2.91–2.85 (m, 2H), 1.44–1.31 (m overlap, 13H), 1.27–1.16 (m, 2H); ^{13}C NMR (CD_3OD): δ = 171.82, 171.66, 161.26, 158.44, 145.79, 144.61, 139.80, 133.26, 131.06, 130.00, 129.85, 129.39, 127.35, 120.68, 119.83, 117.46, 113.27, 109.32, 107.19, 79.78, 69.76, 43.90, 41.18, 40.33, 36.69, 30.53, 30.00, 28.79, 25.03; ESI-MS (*m/z*): 575.5 $[M + H]^+$; HRMS (EI) calcd for $C_{33}H_{42}N_4O_5$, 574.31551, found, 574.31457; HPLC: purity 99% at 254 nm, t_R: 21.9 min.

(*S*)-*N*-(2-{[4-(3,6-Dioxopiperazin-2-yl)butyl]amino}-2-oxoethyl)-2-[(3-phenethoxyphenyl)amino]benzamide (43). White solid, crystallized from EtOAc/MeOH (8/2) (0.050 g, 0.090 mmol, 49%); R*f* = 0.34 (EtOAc:MeOH = 8:2); m.p. 174–176°C; ^{1}H NMR (DMSO-d_6): δ = 9.55 (s, 1H), 8.71 (t, 1H, *J* = 5.9 Hz), 8.15 (s, 1H), 7.98–7.91 (m overlap, 2H), 7.69 (d, 1H, *J* = 7.6 Hz), 7.37–7.15 (m overlap, 8H), 6.88–6.82 (m, 1H), 6.73–6.69 (m overlap 2H), 6.53 (dd, 1H, *J* = 8.3, 1.5 Hz), 4.16 (t, 2H, *J* = 7.0 Hz), 3.82 (d, 2H, *J* =

5.7 Hz), 3.76–3.62 (m overlap, 3H), 3.09–3.00 (m overlap 4H), 1.73–1.61 (m, 2H), 1.45–1.25 (m overlap, 4H); ^{13}C NMR (DMSO-d_6): δ = 168.90, 168.58, 167.99, 166.13, 159.43, 143.87, 142.95, 138.39, 131.85, 130.10, 128.94, 128.28 (2C), 126.24, 119.15, 118.27, 115.52, 111.53, 107.94, 105.32, 68.02, 54.09, 44.29, 42.36, 38.54, 34.93, 32.47, 28.83, 21.57; ESI-MS (*m/z*): 558.5 [M + H]$^+$; HRMS (ESI) calcd for $C_{31}H_{35}N_5O_5Na^+$, 580.2530, found, 580.2527; HPLC: purity 98% at 254 nm, t_R: 16.3 min.

Synthesis of (*S*)-*N*-(2-{[4-(3,6-dioxopiperazin-2-yl)butyl]amino}-2-thioxoethyl)-2-[(3-phenethoxyphenyl)amino]benzamide (53). Step 1: preparation of (*S*)-methyl 6-{[(benzyloxy)carbonyl]amino}-2-[(*tert*-butoxycarbonyl)amino]hexanoate (44). To a solution of **13** (1.0 g, 2.6 mmol) and K_2CO_3 (0.724 g, 5.26 mmol) in dry acetone (10 mL) was added MeI (0.33 mL, 5.26 mmol). The mixture was heated at 65°C under an N_2 atmosphere for 26 h, then filtered, and the filtrate was evaporated under reduced pressure. The residue was extracted with $CHCl_3$ and the organic layer was washed with water, saturated aqueous $NaHCO_3$ solution, water, and brine, dried over Na_2SO_4 and evaporated under vacuum to furnish a colourless oil (1.02 g, 2.59 mmol, 98%); ^{1}H NMR ($CDCl_3$): δ = 7.35–7.29 (m, 5H), 5.08 (s br, 3H), 4.86 (s br, 1H), 4.27 (q br, 1H, *J* = 7.9 Hz), 3.72 (s, 3H), 3.17 (q, 2H, *J* = 6.6 Hz), 1.86–1.73 (m, 1H), 1.69–1.59 (m, 1H), 1.57–1.47 (m, 2H), 1.42 (s, 9H), 1.42–1.30 (m, 2H); ^{13}C NMR ($CDCl_3$): δ = 173.21, 156.47, 155.45, 136.63, 128.48, 128.06, 79.92, 66.62, 53.20, 52.22, 40.64, 32.35, 29.38, 28.30, 22.39 (one C_{ar} overlapped); ESI-MS (*m/z*): 294.9 [M + H]$^+$.

Step 2: preparation of (*S*)-methyl 6-amino-2-[(*tert*-butoxycarbonyl)amino]hexanoate (45). Compound **45** was prepared from **44** by using a similar procedure to that described for the preparation of **8** (Step 2); colourless oil (0.55 g, 2.11 mmol, 93 %); ^{1}H NMR ($CDCl_3$): δ = 5.34 (d br, 1H), 4.25 (s br, 1H), 3.74 (s, 3H), 3.02 (s br, 2H), 1.80–1.59 (m br, 4H), 1.43 (s br,

11H); ^{13}C NMR ($CDCl_3$): δ = 173.24, 155.61, 79.93, 53.35, 52.33, 39.68, 31.92, 28.31, 27.07, 22.46; ESI-MS (*m*/*z*): 260.9 $[M + H]^+$.

Step 3: preparation of (*S*)-methyl 6-[2-({[(9*H*-fluoren-9-yl)methoxy]carbonyl}amino)acetamido]-2-[(*tert*-butoxycarbonyl)amino]hexanoate (46). To a solution of *N*-Fmoc glycine (0.90 g, 3.0 mmol) in DMF/CH_2Cl_2 (1:1, 20 mL) were added COMU® (1.56 g, 3.7 mmol) and *i*-Pr_2NEt (0.64 mL, 3.7 mmol) on an ice bath. The reaction mixture was stirred for 5 min and then a solution of **45** (0.79 g, 3.0 mmol) in CH_2Cl_2 (5 mL) was added. Stirring was continued on ice for 1 h and then at room temperature for 4 h. The reaction solvent was removed under vacuum, and the residue was dissolved in EtOAc. The organic solution was washed with water and brine, and dried over anhydrous Na_2SO_4. The organic phase was evaporated under vacuum and the residue was purified by column chromatography (*n*-hexane:EtOAc = 2:1) to afford a colourless sticky oil (1.52 g, 2.82 mmol, 93%); R*f* = 0.25 (*n*-hexane:EtOAc = 2:1); ^{1}H NMR ($CDCl_3$): δ = 7.75 (d, 2H, *J* = 7.5 Hz), 7.58 (d, 2H, *J* = 7.4 Hz), 7.39 (t, 2H, *J* = 7.2 Hz), 7.29 (td, 2H, *J* = 7.4, 1.2 Hz), 6.33 (s br, 1H), 5.73 (s br, 1H), 5.18 (d br, 1H, *J* = 8.3 Hz), 4.41 (d, 2H, *J* = 6.93 Hz), 4.29–4.18 (m, 1H), 4.21 (t, 1H, *J* = 6.9 Hz), 3.82 (d, 2H, *J* = 6.0 Hz), 3.71 (s, 3H), 3.24 (q, 2H, *J* = 6.6 Hz), 1.84–1.72 (m, 1H), 1.68–1.59 (m, 1H), 1.56–1.45 (m, 2H), 1.43 (s, 9H), 1.43–1.31 (m, 2H); ^{13}C NMR ($CDCl_3$): δ = 173.21, 169.03, 156.70, 155.54, 143.74, 141.30, 127.75, 127.08, 125.03, 119.99, 80.01, 67.17, 53.20, 52.26, 47.13, 44.56, 39.10, 32.32, 28.81, 28.32, 22.53; ESI-MS (*m*/*z*): 540.2 $[M + H]^+$.

Step 4: preparation of (*S*)-methyl 6-[2-({[(9*H*-fluoren-9-yl)methoxy]carbonyl}amino)ethanethioamido]-2-[(*tert*-butoxycarbonyl)amino]hexanoate (47). A solution of **46** (0.68 g, 1.28 mmol) and Lawesson's reagent (0.26 g, 0.64 mmol) in anhydrous toluene (10 mL) was heated at 60°C for 3 h. The reaction solvent was removed under vacuum and the residue was purified by

column chromatography (*n*-hexane:EtOAc = 2:1) to furnish a colourless gum (0.60 g, 1.08 mmol, 86%); R*f* = 0.19 (*n*-hexane:EtOAc = 2:1); ^{1}H NMR ($CDCl_3$): δ = 8.34 (s br, 1H), 7.74 (d, 2H, *J* = 7.5 Hz), 7.57 (d, 2H, *J* = 7.4 Hz), 7.38 (t, 2H, *J* = 7.2 Hz), 7.28 (td, 2H, *J* = 7.4, 1.2 Hz), 5.96 (t br, 1H, *J* = 5.6 Hz), 5.17 (d br, 1H, *J* = 8.5 Hz), 4.40 (d, 2H, *J* = 7.0 Hz), 4.28–4.20 (m, 1H), 4.20 (t, 1H, *J* = 6.9 Hz), 4.16 (d, 2H, *J* = 6.0 Hz), 3.70 (s, 3H), 3.65–3.58 (m, 2H), 1.83–1.72 (m, 1H), 1.66–1.53 (m, 3H), 1.47–1.33 (m, 2H), 1.42 (s, 9H); ^{13}C NMR ($CDCl_3$): δ = 199.10, 173.14, 156.94, 155.56, 143.62, 141.30, 127.81, 127.12, 125.04, 120.04, 80.10, 67.43, 53.14, 52.32, 52.01, 47.06, 44.42, 32.14, 28.33, 27.16, 22.72; ESI-MS (*m*/*z*): 556.2 $[M + H]^+$.

Step 5: preparation of (*S*)-6-[2-({[(9*H*-fluoren-9-yl)methoxy]carbonyl}amino)ethanethioamido]-2-[(*tert*-butoxycarbonyl)amino]hexanoic acid (48). A solution of **47** (0.44 g, 0.79 mmol) and Me_3SnOH (0.72 g, 3.97 mmol) in 1,2-dichloroethane (13 mL) was heated at 60 °C for 10 h. $CHCl_3$ was added, and the organic phase was washed with 0.1 M aqueous HCl solution, water, and brine, dried over Na_2SO_4, and evaporated under vacuum. The resulting crude product was purified by column chromatography ($CHCl_3$:MeOH = 100:1) to furnish a colourless gum (0.30 g, 0.55 mmol, 70%); R*f* = 0.11 ($CHCl_3$:MeOH, 40:1); ^{1}H NMR ($CDCl_3$): δ = 8.42 (s br, NH), 7.73 (d, 2H, *J* = 7.5 Hz), 7.55 (d, 2H, *J* = 7.4 Hz), 7.37 (t, 2H, *J* = 7.5 Hz), 7.27 (td, 2H, *J* = 7.4, 1.2 Hz), 5.29 (d br, 1H, *J* = 5.1), 4.38 (d, 2H, *J* = 7.0 Hz), 4.29–4.18 (m, 1H), 4.18 (t, 1H, *J* = 7.1 Hz), 4.17 (d, 2H, *J* = 6.9 Hz), 3.67–3.59 (m, 2H), 1.83–1.75 (m, 1H), 1.72–1.58 (m, 3H), 1.41 (s br, 11H); ^{13}C NMR ($CDCl_3$): δ = 199.09, 175.77, 157.14, 155.92, 143.55, 141.29, 127.83, 127.14, 125.05, 120.05, 80.47, 67.64, 53.25, 51.78, 46.99, 45.33, 31.75, 28.31, 26.95, 22.65; ESI-MS (*m*/*z*): 542.2 $[M + H]^+$.

Step 6: preparation of (*S*)-ethyl 12-[(*tert*-butoxycarbonyl)amino]-1-(9*H*-fluoren-9-yl)-3,13-dioxo-6-thioxo-2-oxa-4,7,14-triazahexadecan-16-oate (49). Compound **49** was

prepared from **49** and glycine ethyl ester by using a similar procedure to that described for the preparation of **46**; colourless sticky oil (0.22 g, 0.35 mmol, 88%); R*f* = 0.17 (*n*-hexane:EtOAc = 1:1); ^{1}H NMR ($CDCl_3$): δ = 8.53 (s br, 1H), 7.74 (d, 2H, *J* = 7.5 Hz), 7.58 (d, 2H, *J* = 7.4 Hz), 7.37 (t, 2H, *J* = 7.5 Hz), 7.30 (td, 2H, *J* = 7.5, 1.3 Hz), 7.01 (s br, 1H), 6.14 (s br, 1H), 5.41 (d br, 1H, *J* = 8.1), 4.39 (d, 2H, *J* = 7.1 Hz), 4.20 (t, 1H, *J* = 7.1 Hz), 4.20–4.06 (m, 3H), 4.13 (q, 2H, *J* = 7.1 Hz), 4.04 (dd, 1H, *J* = 18.0, 5.7 Hz), 3.90 (dd, 1H, *J* = 18.0, 5.4 Hz), 3.72–3.64 (m, 2H), 1.87–1.75 (m, 1H), 1.70–1.58 (m, 3H), 1.47–1.41 (m, 2H), 1.41 (s br, 9H), 1.22 (t, 3H, *J* = 7.1 Hz); ^{13}C NMR ($CDCl_3$): δ = 199.19, 172.63, 169.96, 156.84, 155.76, 143.67, 141.28, 127.78, 127.11, 125.08, 120.01, 80.23, 67.35, 61.60, 54.06, 51.74, 47.06, 45.33, 41.23, 32.11, 28.33, 26.96, 22.58, 14.07; ESI-MS (*m*/*z*): 627.3 $[M + H]^+$.

Step 7: preparation of (*S*)-1-(9*H*-fluoren-9-yl)-3,13,16-trioxo-6-thioxo-2,17-dioxa-4,7,14-triazanonadecan-12-aminium trifluoroacetate (50). Compound **50** was prepared from **49** by using a similar procedure to that described for the preparation of **17** (step 2); pale yellow sticky gum (0.22 g, 0.34 mmol, 93%); ^{1}H NMR ($CDCl_3$): δ = 8.85 (s br, 1H), 8.11 (s br, 4H), 7.69 (d, 2H, *J* = 7.5 Hz), 7.53 (d, 2H, *J* = 7.6 Hz), 7.33 (t, 2H, *J* = 7.4 Hz), 7.24 (t, 2H, *J* = 7.2 Hz), 6.24 (s br, 1H), 4.29 (d, 2H, *J* = 7.1 Hz), 4.20–3.99 (m, 3H), 4.15 (t, 1H, *J* = 6.9 Hz), 4.05 (q, 2H, *J* = 7.0 Hz), 3.95 (d br, 1H, *J* = 15.8 Hz), 3.84 (d br, 1H, *J* = 15.9 Hz), 3.61 (s br, 2H), 1.86 (s br, 2H), 1.61 (s br, 2H), 1.43 (s br, 2H), 1.15 (t, 3H, *J* = 7.0 Hz); ^{13}C NMR ($CDCl_3$): δ = 199.23, 169.84, 156.99, 143.61, 141.22, 127.80, 127.12, 125.09, 120.00, 67.46, 61.92, 53.36, 51.00, 46.92, 44.84, 41.31, 30.83, 26.47, 21.43, 13.88 (one C_{ar} overlapped); ESI-MS (*m*/*z*): 527.2 $[M + H]^+$.

Step 8: preparation of (*S*)-(9*H*-fluoren-9-yl)methyl (2-{[4-(3,6-dioxopiperazin-2-yl)butyl)amino]-2-thioxoethyl}carbamate (51). Compound **51** was prepared from **50** by using a similar procedure to that described for the preparation of compound **17** (step 3); white amorphous solid (0.29 g, 0.60 mmol, 63%). m.p. 141–143°C; ^{1}H NMR ($CDCl_3$/drop

CD_3OD): δ = 7.77 (d, 2H, *J* = 7.4 Hz), 7.61 (d, 2H, *J* = 6.6 Hz), 7.41 (t, 2H, *J* = 7.3 Hz), 7.31 (td, 2H, *J* = 7.5, 1.2 Hz), 6.50 (s br, 1H), 4.43 (d, 2H, *J* = 6.7 Hz), 4.23 (t, 1H, *J* = 6.8 Hz), 4.12 (s br, 2H), 3.94 (d, 1H, *J* = 17.8 Hz), 3.88 (d, 1H, *J* = 18.1 Hz), 3.76–3.60 (m, 2H), 1.89–1.82 (m, 2H), 1.73–1.65 (m, 2H), 1.51–1.36 (m, 2H); ^{13}C NMR ($CDCl_3$/drop CD_3OD): δ = 199.28, 168.64, 166.48, 143.64, 141.24, 127.73, 127.06, 124.97, 119.94, 67.19, 54.56, 51.35, 47.02, 44.81, 44.44, 32.86, 26.78, 21.42 (one C_{ar} overlapped); ESI-MS (*m*/*z*): 481 $[M + H]^+$.

Step 9: preparation of (*S*)-2-amino-*N*-[4-(3,6-dioxopiperazin-2-yl)butyl]ethanethioamide (52). To a stirred suspension of **52** (0.20 g, 0.42 mmol) in dry CH_2Cl_2 (18 mL) was added piperidine (3.6 mL). The reaction mixture was stirred at room temperature for 30 min, and then evaporated *in vacuo*. The crude product was washed with $CHCl_3$ to furnish a brownish amorphous solid; 0.075 g, 0.29 mmol, 69%; m.p. 169–171°C (dec.); ^1H NMR (CD_3OD): δ = 4.00 (dd, 1H, *J* = 17.8, 1.1 Hz), 3.95 (dd, 1H, *J* = 6.1, 1.2 Hz), 3.86 (dd, 1H, *J* = 17.8, 1.1 Hz), 3.69 (t, 2H, *J* = 7.0 Hz), 3.55 (s, 2H), 1.96–1.81 (m, 2H), 1.80–1.67 (quint., 2H), 1.53–1.42 (m, 2H); ESI-MS (*m*/*z*): 258.9 $[M + H]^+$.

Step 10: preparation of (*S*)-*N*-(2-{[4-(3,6-dioxopiperazin-2-yl)butyl]amino}-2-thioxoethyl)-2-[(3-phenethoxyphenyl)amino]benzamide (53). Compound **53** was prepared from **52** and **18** by using a similar procedure to that described for the preparation of compound **46**; yellowish sticky gum (0.071 g, 0.12 mmol, 70 %). R*f* = 0.15 (EtOAc:MeOH = 25:1); ^1H NMR ($CDCl_3$): δ = 9.06 (s br, 1H), 8.89 (s br, 1H), 7.71 (t br, 1H, *J* = 5.6 Hz), 7.56 (d, 1H, *J* = 7.6 Hz), 7.36–7.14 (m, 6H), 7.17 (t, 1H, *J* = 8.0 Hz), 6.83 (s br, 1H), 6.80 (d, 1H, *J* = 8.0 Hz), 6.72 (d, 1H, *J* = 8.8 Hz), 6.70 (s, 1H), 6.55 (dd, 1H, *J* = 8.3, 1,6 Hz), 6.31 (s br, 1H), 4.43 (dd, 1H, *J* = 16.5, 6.0 Hz), 4.33 (dd, 1H, *J* = 16.5, 6.0 Hz), 4.14 (t, 2H, *J* = 7.1 Hz), 3.90 (s br, 1H), 3.83 (s br, 2H), 3.77 (dd, 1H, *J* = 13.5, 6.2 Hz), 3.62 (dd, 1H, *J* = 13.5, 6.2 Hz), 3.07 (t, 2H, *J* = 7.1 Hz), 1.80 (m br, 2H), 1.66 (s br, 2H), 1.35 (m, 2H); ^{13}C NMR

($CDCl_3$): δ = 199.64, 170.38, 168.00, 166.17, 159.91, 145.30, 142.37, 138.24, 132.87, 130.15, 129.02, 128.48, 126.50, 118.70, 117.72, 116.46, 113.08, 108.69, 107.01. 68.70, 54.58, 51.11, 44.78, 44.67, 35.76, 32.40, 26.83, 20.82 (one C_{ar} overlapped); ESI-MS (*m*/*z*): 574.3 $[M + H]^+$; HRMS (ESI) calcd for $C_{31}H_{35}N_5O_4Na^+$, 596.2302, found, 596.2306; HPLC: purity 98 % at 254 nm, t_R: 17.7 min.

SIRT1-3 and SIRT5 Assay.[75] Fluor de Lys assays were performed according to the method described in the assay kit sheets AK-555, 556, 557, and 513. The assays were carried out using acetylated substrates at concentrations of 25 μM (BML-KI177-0005 for SIRT1 and BML-KI179-0005 for SIRT2 and SIRT3) or 10 μM (BML-KI590-0050 for SIRT5); SIRT1 0.5–1 U/well (BML-SE239-0100), SIRT2 4–6 U/well (BML SE-251-0500), SIRT3 4 U/well (BML-SE270-0500), SIRT5 8 U/well (BML-SE555-9090), and NAD^+ 1 mM for SIRT1, SIRT2, and SIRT5, 1.8 mM for SIRT3. Developer II solution (BML-KI176-1250)/nicotinamide 1 mM (BML-KI283-0500) and sirtuin buffer were provided as part of the kit. DMSO (purchased from Nacalai) was used at a final concentration of 2%. An aliquot of 10 μL of test compound in buffer/DMSO was added quickly to each selected well (buffer/DMSO was added to the control and blank wells), followed by 25 μL of buffer solution containing the substrate/NAD^+. After gentle mixing, the reaction was started by adding 15 μL of the diluted enzyme (15 μL of buffer was added to the blank wells). The reaction mixtures were incubated for 3 h at 30°C without rotation. Then, 50 μL of a stop solution containing Fluor de Lys Developer II/nicotinamide was added to each well and the fluorescence was measured for 0–30 min at 30°C using an ARVO™ X3 plate reader (λ_{ex} = 355 nm; λ_{em} = 460 nm). IC_{50} values were determined from three independent measurements, affording a total of at least 21 data points. All data points were included in the IC_{50} calculation using GraFit 7.03, in which three independent curves were generated.

SIRT2 substrate competition analysis of 43 and 53. The assay followed the procedure described for the SIRT2 assay (*vide supra*), except for the following changes: reaction time = 45 min; [NAD^+] = 2 mM; [substrate] = 100, 150, 200, and 400 μM.

Molecular Modeling.[75] The crystal structure SIRT2-NCO-90 (PDB code: 5Y5N) was prepared for docking simulation using Chimera 1.10.2[81] (default) saved as pdb and uploaded to Molegro Virtual Docker 6.0. Docked compounds were prepared with ChemBioDraw ultra 12.0, imported in Chem3D, and saved as Sybil mol2 files. These files were uploaded to Molegro and prepared using default parameters, in which charges were added, and Nelder-Mead (simplex) minimization with 2000 iterations was performed. The docking procedure was validated by redocking the crystallized SIRT2 inhibitor NCO-90 with an RMSD value of 0.70 Å. Plants Score[GRID] and MolDock Optimizer were chosen as the scoring function and algorithm, respectively. Displaceable water molecule evaluation was applied to HOH3, HOH4, and HOH11. A box containing the binding site with coordinates X: 48.95, Y: 56.74, Z: 23.46 and radius: 15 was created to guide the docking simulation. The number of runs was set to 40, population size to 100, and 10 poses were retained for each ligand. Each pose was manually inspected and selected or discarded considering both ranking position and correct placement in the binding site (for example: inversion of binding mode by 180 degree rotation of the anthranylamide moiety was considered unsatisfactory). Selected poses were refined with the ligand energy inspector tool, in which ligand and protein H position were optimized. Figures 2 and 4 were prepared using UCSF Chimera 1.10.2,[81] and ChemDraw Std 13.0.

Mass spectrometric detection of the ADP-ribose conjugate. Reactions were conducted for 5 min at 37°C in 5 μL of a solution containing 1.9 μM SIRT2 (SignalChem), 500 μM NAD^+, and 1 mM **53**, as well as 40 mM sodium phosphate buffer (pH = 7.0) containing 240 mM NaCl, 120 mM imidazole, 0.08 mM phenylmethylsulfonyl fluoride, 0.2 mM

dithiothreitol, 20% glycerol, and 2% DMSO. Controls were measured in the absence of compounds, NAD+ or the enzyme. The reaction mixtures were diluted with 5 μL of water and purified using ZipTip-μC_{18} (Millipore). The fraction eluted with 2 μL of 50% acetonitrile containing α-cyano-4-hydroxycinnamic acid at a concentration of 5 mg/mL was directly subjected to MALDI-TOF MS analysis. MALDI-TOF mass spectra were acquired on an AB SCIEX TOF/TOF™ 5800 (AB SCIEX) in the reflectron negative ion mode.

Cell cultures. MCF-7 cells (RIKEN BRC) were cultured in Dulbecco's modified Eagle's medium (DMEM; Nacalai, #08489-45) containing 10% fetal bovine serum (FBS; SIGMA, #172012), antibiotic-antimycotic mixed stock solution (Nacalai, #09366-44), L-glutamine stock solution (Nacalai, #16948-04), and sodium pyruvate solution (Nacalai, #06977-34) at 37 °C in a humidified atmosphere of 5% CO_2 in air. The Neuro-2a (N2a) cell line was obtained from the Japanese Collection of Research Bioresources (JCRB) Cell Bank, and cultured as reported.[89]

Mass spectrometric analysis of compound 43 in the presence of SIRT2. Compound **43** (1 μM) was incubated with NAD^+ (1 mM) in the presence or absence of SIRT2 (12.8 μM, BML-KI286) for 3 h at 30 °C in assay buffer. Control experiments were conducted using commercially available SIRT2 substrate (Ac-QPKK(Ac)-AMC, BML-KI179)[90] instead of **43**. Reaction mixtures (5 μL) were denatured with 0.2% TFA aqueous solution (5 μL). The mixtures were desalted and concentrated using ZipTip-μC_{18} (Millipore: CH_3CN/H_2O, v/v = 1:1, containing 0.1% formic acid) and subjected to ESI-MS analysis. ESI mass spectra were acquired on an HCT plus instrument (Bruker).

Cell growth assay. MCF-7 cells were plated in 96-well plates (1×10^3 cells/50 μL/well) and incubated at 37 °C under 5% CO_2 in air. After 24 h, test compound solutions (50 μL/well) of varying concentrations in culture medium were added to the cells at 37 °C. The cultures were incubated for 72 h, then 10 μL of AlamarBlue® (AbD Serotec, #BUF012A) was added,

and incubation was continued at 37 °C for 3 h. The fluorescence in each well was measured with an ARVO™ X3 microplate reader (λ_{ex} = 540 nm; λ_{em} = 590 nm). Cell growth (percent) was calculated from the obtained fluorescence readings.

Western Blotting. MCF-7 cells (5×10^5 cells/2 mL/dish) were treated for 24 h with test compounds at the indicated concentrations in the cell culture medium, and then the cells were collected and extracted with SDS buffer. The protein concentrations of the lysates were determined using BCA protein assay. Equivalent amounts of protein from each lysate were resolved in 5–20% SDS-polyacrylamide gels and transferred to poly vinylidene difluoride (PVDF) membranes. The transblotted membranes were blocked with TBS-T containing 5% skimmed milk, and probed with rabbit monoclonal H3K9Ac antibody (CST, #9649) (1:1000 dilution), rabbit polyclonal H3 antibody (Abcam, #ab1791) (1:200000 dilution), mouse monoclonal acetyl-α-tubulin antibody (Sigma, #T6793) (1:2000 dilution), or mouse monoclonal α-tubulin antibody (Sigma, #T8203) (1:2000 dilution) in TBS-T containing 5% skimmed milk. The probed membranes were washed three times with TBS-T, incubated with ECL rabbit IgG, HRP-linked whole antibody (GE Healthcare Life Sciences, #NA934) (1:2500 dilution), or ECL mouse IgG, HRP-linked whole antibody (GE Healthcare Life Sciences, #NA931) (1:2500 or 1:10000 dilution), and washed again three times with TBS-T. The immunoblots were visualized by enhanced chemiluminescence with Immobilon™ Western Chemiluminescent HRP Substrate (Millipore, #WBKLS0500).

Neurite outgrowth assay. N2a cells were plated at a concentration of 1×10^4 cell/mL in DMEM including high glucose, 10% FBS, 100 U/mL penicillin, and 100 μg/mL streptomycin at 37°C in a humidified atmosphere of 5% CO_2 in air. For the differentiation study, the medium was changed to DMEM supplemented with 2% FBS. After incubation with KPM-2, **43**, **53** for 24 h or 48 h, the cell morphology was examined using a microscope (Olympus CKX41) and further analyzed with Photomeasure software (Kenis Ltd.). The

differentiated cells were defined as those with at least one neurite that was longer than twice the diameter of the cell body. The results are expressed as the percentage of differentiated cells relative to the total number of counted cells. These experiments were carried out in triplicate. One-way ANOVA and Dunnett's *post hoc* tests were used to determine the significance of differences among the groups.

ASSOCIATED CONTENT

Supporting Information

The Supporting Information is available free of charge on the ACS Publications website at DOI: 10.1021/acs.jmed-chem.XXXXXXX.

Figures S1–S6, HPLC data and NMR charts of synthetic compounds (PDF)

Molecular formula strings (CSV)

Docking poses of compounds **21**, **23**, **24**, **26**, **35**, **36**, and **38** in the SIRT2 crystal structure (PDB)

Primary Data

PDB ID code: 4Y6O (X-ray structure of SIRT2/myristoylated substrate peptide complex), 4RMI (SIRT2/SirReal2 complex), 5Y5N (SIRT2/NCO-90 complex). The structure of SIRT2/NCO-90 complex was used for the docking studies. Authors will release the atomic coordinates and experimental data upon article publication.

AUTHOR INFORMATION

Corresponding Author. * To whom correspondence should be addressed: T.S. suzukit@koto.kpu-m.ac.jp

Notes

The authors declare no competing financial interest.

ACKNOWLEDGMENT

The authors would like to thank Dr. Yasunao Hattori, Prof. Kenichi Akaji, Dr. Naoya Ieda, Dr. Mitsuyasu Kawaguchi, and Prof. Hidehiko Nakagawa for their technical support. This work was supported in part by the JST CREST program (T.S.; JPMJCR14L2), the JST A-step program (Y.I.; 957908), and a JSPS fellowship for foreign researchers (P.M.; E.E.E.).

ABBREVIATIONS

AceCS, acetyl-CoA synthetase; c-Myc, cellular myelocytomatosis oncogene; COMU, 1-[(1-(cyano-2-ethoxy-2-oxoethylideneaminooxy) dimethylaminomorpholino)]uronium hexafluorophosphate; DMEM, Dulbecco's modified Eagle's medium; EDCI, 1-ethyl-3-(3-dimethylaminopropyl)carbodiimide; GI_{50}, half-maximum growth inhibitory concentration; GLUT, glucose transporter; HDAC, histone deacetylase; HIC, hypermethylated in cancer; HIF, hypoxia inducible factor; HOBt, 1-hydroxybenzotriazole; IDH, isocitrate dehydrogenase; JNK, c-jun N-terminal kinase; KDM, lysine demethylase; miR, microRNA; PAIN, pan assay interference compound; PEPCK, phosphoenolpyruvate carboxykinase; N2a, Neuro 2a; PGC, PPARγ co-activator; PVDF, poly vinylidene difluoride; RAS, rat sarcoma;

SIRT, sirtuin; SOD, superoxide dismutase; UCP, uncoupling protein; XPhos, 2-dicyclohexylphosphino-2',4',6'-triisopropyl biphenyl.

REFERENCES

(1) Klar, A. J.; Fogel, S.; Macleod, K. MAR1-a regulator of the HMa and HMα loci in Saccharomyces cerevisiae. *Genetics* **1979**, *93*, 37–50.

(2) Frye, R. A. Phylogenetic classification of prokaryotic and eukaryotic Sir2-like proteins. *Biochem. Biophys. Res. Commun.* **2000**, *273*, 793–798.

(3) Landry, J.; Slama, J. T.; Sternglanz, R. Role of NAD^+ in the deacetylase activity of the SIR2-like proteins. *Biochem. Biophys. Res. Commun.* **2000**, *278*, 685–690.

(4) Smith, J. S.; Brachmann, C. B.; Celic, I.; Kenna, M. A.; Muhammad, S.; Starai, V. J.; Avalos, J. L.; Escalante-Semerena, J. C.; Grubmeyer, C.; Wolberger, C.; Boeke, J. D. A phylogenetically conserved NAD^+-dependent protein deacetylase activity in the Sir2 protein family. *Proc. Natl. Acad. Sci. U. S. A.* **2000**, *97*, 6658–6663.

(5) Feldman, J. L.; Baeza, J.; Denu, J. M. Activation of the protein deacetylase SIRT6 by long-chain fatty acids and widespread deacylation by mammalian sirtuins. *J. Biol. Chem.* **2013**, *288*, 31350–31356.

(6) Teng, Y.-B.; Jing, H.; Aramsangtienchai, P.; He, B.; Khan, S.; Hu, J.; Lin, H.; Hao, Q. Efficient demyristoylase activity of SIRT2 revealed by kinetic and structural studies. *Sci. Rep.* **2015**, *5*, 8529.

(7) Tong, Z.; Wang, M.; Wang, Y.; Kim, D. D.; Grenier, J. K.; Cao, J.; Sadhukhan, S.; Hao, Q.; Lin, H. SIRT7 is an RNA-activated protein lysine deacylase. *ACS Chem. Biol.* **2017**, *12*, 300–310.

(8) Jin, J.; He, B.; Zhang, X.; Lin, H.; Wang, Y. SIRT2 reverses 4-oxononanoyl lysine modification on histones. *J. Am. Chem. Soc.* **2016**, *138*, 12304–12307.

(9) Du, J.; Zhou, Y.; Su, X.; Yu, J. J.; Khan, S.; Jiang, H.; Kim, J.; Woo, J.; Kim, J. H.; Choi, B. H.; He, B.; Chen, W.; Zhang, S.; Cerione, R. A.; Auwerx, J.; Hao, Q.; Lin, H.

Sirt5 is a NAD-dependent protein lysine demalonylase and desuccinylase. *Science* **2011**, *334*, 806–809.

(10) Li, L.; Shi, L.; Yang, S.; Yan, R.; Zhang, D.; Yang, J.; He, L.; Li, W.; Yi, X.; Sun, L.; Liang, J.; Cheng, Z.; Shi, L.; Shang, Y.; Yu, W. SIRT7 is a histone desuccinylase that functionally links to chromatin compaction and genome stability. *Nat. Commun.* **2016**, *7*, 12235.

(11) Huang, H.; Zhang, D.; Wang, Y.; Perez-Neut, M.; Han, Z.; Zheng, Y. G.; Hao, Q.; Zhao, Y. Lysine benzoylation is a histone mark regulated by SIRT2. *Nat. Commun.* **2018**, *9*, 3374.

(12) Michishita, E.; Park, J. Y.; Burneskis, J. M.; Barrett, J. C.; Horikawa, I. Evolutionarily conserved and nonconserved cellular localizations and functions of human SIRT proteins. *Mol. Biol. Cell* **2005**, *16*, 4623–4635.

(13) Guarente, L. Sirtuins as potential targets for metabolic syndrome. *Nature* **2006**, *444*, 868–874.

(14) Baur, J. A.; Ungvari, Z.; Minor, R. K.; Le Couteur, D. G.; de Cabo, R. Are sirtuins viable targets for improving healthspan and lifespan? *Nat. Rev. Drug Discov.* **2012**, *11*, 443–461.

(15) Picard, F.; Kurtev, M.; Chung, N.; Topark-Ngarm, A.; Senawong, T.; Machado De Oliveira, R.; Leid, M.; McBurney, M. W.; Guarente, L. Sirt1 promotes fat mobilization in white adipocytes by repressing PPAR-γ. *Nature* **2004**, *429*, 771–776.

(16) Rodgers, J. T.; Lerin, C.; Haas, W.; Gygi, S. P.; Spiegelman, B. M.; Puigserver, P. Nutrient control of glucose homeostasis through a complex of PGC-1α and SIRT1. *Nature* **2005**, *434*, 113–118.

(17) Rodgers, J. T.; Lerin, C.; Gerhart-Hines, Z.; Puigserver, P. Metabolic adaptations through the PGC-1α and SIRT1 pathways. *FEBS Lett.* **2008**, *582*, 46–53.

(18) Bordone, L.; Motta, M. C.; Picard, F.; Robinson, A.; Jhala, U. S.; Apfeld, J.; McDonagh, T.; Lemieux, M.; McBurney, M.; Szilvasi, A.; Easlon, E. J.; Lin, S.-J.; Guarente, L. Sirt1 regulates insulin secretion by repressing UCP2 in pancreatic β cells. *PLoS Biol.* **2006**, *4*, e31.

(19) Palacios, O. M.; Carmona, J. J.; Michan, S.; Chen, K. Y.; Manabe, Y.; Ward, J. L.; Goodyear, L. J.; Tong, Q. Diet and exercise signals regulate SIRT3 and activate AMPK and PGC-1α in skeletal muscle. *Aging* **2009**, *1*, 771–783.

(20) Kincaid, B.; Bossy-Wetzel, E. Forever young: SIRT3 a shield against mitochondrial meltdown, aging, and neurodegeneration. *Front. Aging Neurosci.* **2013**, *5*, 48.

(21) Huang, J.-Y.; Hirschey, M. D.; Shimazu, T.; Ho, L.; Verdin, E. Mitochondrial sirtuins. *Biochim. Biophys. Acta* **2010**, *1804*, 1645–1651.

(22) Schwer, B.; Bunkenborg, J.; Verdin, R. O.; Andersen, J. S.; Verdin, E. Reversible lysine acetylation controls the activity of the mitochondrial enzyme acetyl-CoA synthetase 2. *Proc. Natl. Acad. Sci. U. S. A.* **2006**, *103*, 10224–10229.

(23) Chen, Y.; Zhang, J.; Lin, Y.; Lei, Q.; Guan, K.-L.; Zhao, S.; Xiong, Y. Tumour suppressor SIRT3 deacetylates and activates manganese superoxide dismutase to scavenge ROS. *EMBO Rep.* **2011**, *12*, 534–541.

(24) Qiu, X.; Brown, K.; Hirschey, M. D.; Verdin, E.; Chen, D. Calorie restriction reduces oxidative stress by SIRT3-mediated SOD2 activation. *Cell Metab.* **2010**, *12*, 662–667.

(25) Yu, W.; Dittenhafer-Reed, K. E.; Denu, J. M. SIRT3 protein deacetylates isocitrate dehydrogenase 2 (IDH2) and regulates mitochondrial redox status. *J. Biol. Chem.* **2012**, *287*, 14078–14086.

(26) Lerrer, B.; Cohen, H. Y. The guardian: metabolic and tumour-suppressive effects of SIRT6. *EMBO J.* **2013**, *32*, 7–8.

(27) Sebastián, C.; Zwaans, B. M. M.; Silberman, D. M.; Gymrek, M.; Goren, A.; Zhong, L.; Ram, O.; Truelove, J.; Guimaraes, A. R.; Toiber, D.; Cosentino, C.; Greenson, J. K.; MacDonald, A. I.; McGlynn, L.; Maxwell, F.; Edwards, J.; Giacosa, S.; Guccione, E.; Weissleder, R.; Bernstein, B. E.; Regev, A.; Shiels, P. G.; Lombard, D. B.; Mostoslavsky, R. The histone deacetylase SIRT6 is a tumor suppressor that controls cancer metabolism. *Cell* **2012**, *151*, 1185–1199.

(28) Zhong, L.; D'Urso, A.; Toiber, D.; Sebastian, C.; Henry, R. E.; Vadysirisack, D. D.; Guimaraes, A.; Marinelli, B.; Wikstrom, J. D.; Nir, T.; Clish, C. B.; Vaitheesvaran, B.; Iliopoulos, O.; Kurland, I.; Dor, Y.; Weissleder, R.; Shirihai, O. S.; Ellisen, L. W.; Espinosa, J. M.; Mostoslavsky, R. The histone deacetylase Sirt6 regulates glucose homeostasis via Hif1α.*Cell* **2010**, *140*, 280–293.

(29) Maxwell, M. M.; Tomkinson, E. M.; Nobles, J.; Wizeman, J. W.; Amore, A. M.; Quinti, L.; Chopra, V.; Hersch, S. M.; Kazantsev, A. G. The sirtuin 2 microtubule deacetylase is an abundant neuronal protein that accumulates in the aging CNS. *Hum. Mol. Genet.* **2011**, *20*, 3986–3996.

(30) Jayasena, T.; Poljak, A.; Braidy, N.; Zhong, L.; Rowlands, B.; Muenchhoff, J.; Grant, R.; Smythe, G.; Teo, C.; Raftery, M.; Sachdev, P. Application of targeted mass spectrometry for the quantification of sirtuins in the central nervous system. *Sci. Rep.* **2016**, *6*, 35391.

(31) Di Fruscia, P.; Zacharioudakis, E.; Liu, C.; Moniot, S.; Laohasinnarong, S.; Khongkow, M.; Harrison, I. F.; Koltsida, K.; Reynolds, C. R.; Schmidtkunz, K.; Jung, M.; Chapman, K. L.; Steegborn, C.; Dexter, D. T.; Sternberg, M. J. E.; Lam, E. W.-F.; Fuchter, M. J. The discovery of a highly selective 5,6,7,8-tetrahydrobenzo[4,5]thieno[2,3-D]pyrimidin-4(3H)-one SIRT2 inhibitor that is neuroprotective in an in vitro Parkinson's disease model. *ChemMedChem* **2015**, *10*, 69–82.

(32) Taylor, D. M.; Balabadra, U.; Xiang, Z.; Woodman, B.; Meade, S.; Amore, A.; Maxwell, M. M.; Reeves, S.; Bates, G. P.; Luthi-Carter, R.; Lowden, P. A. S.; Kazantsev, A. G. A brain-permeable small molecule reduces neuronal cholesterol by inhibiting activity of sirtuin 2 deacetylase. *ACS Chem. Biol.* **2011**, *6*, 540–546.

(33) Chopra, V.; Quinti, L.; Kim, J.; Vollor, L.; Narayanan, K. L.; Edgerly, C.; Cipicchio, P. M.; Lauver, M. A.; Choi, S. H.; Silverman, R. B.; Ferrante, R. J.; Hersch, S.; Kazantsev, A. G. The sirtuin 2 inhibitor AK-7 is neuroprotective in Huntington's disease mouse models. *Cell Rep.* **2012**, *2*, 1492–1497.

(34) Outeiro, T. F.; Kontopoulos, E.; Altmann, S. M.; Kufareva, I.; Strathearn, K. E.; Amore, A. M.; Volk, C. B.; Maxwell, M. M.; Rochet, J.-C.; McLean, P. J.; Young, A. B.; Abagyan, R.; Feany, M. B.; Hyman, B. T.; Kazantsev, A. G. Sirtuin 2 inhibitors rescue α-synuclein-mediated toxicity in models of Parkinson's disease. *Science* **2007**, *317*, 516–519.

(35) Chen, X.; Wales, P.; Quinti, L.; Zuo, F.; Moniot, S.; Herisson, F.; Rauf, N. A.; Wang, H.; Silverman, R. B.; Ayata, C.; Maxwell, M. M.; Steegborn, C.; Schwarzschild, M. A.; Outeiro, T. F.; Kazantsev, A. G. The sirtuin-2 inhibitor AK7 is neuroprotective in models of Parkinson's disease but not amyotrophic lateral sclerosis and cerebral ischemia. *PLoS One* **2015**, *10*, e0116919.

(36) Quinti, L.; Casale, M.; Moniot, S.; Pais, T. F.; Van Kanegan, M. J.; Kaltenbach, L. S.; Pallos, J.; Lim, R. G.; Naidu, S. D.; Runne, H.; Meisel, L.; Rauf, N. A.; Leyfer, D.; Maxwell, M. M.; Saiah, E.; Landers, J. E.; Luthi-Carter, R.; Abagyan, R.; Dinkova-Kostova, A. T.; Steegborn, C.; Marsh, J. L.; Lo, D. C.; Thompson, L. M.; Kazantsev, A. G. SIRT2- and NRF2-targeting thiazole-containing compound with therapeutic activity in Huntington's disease models. *Cell Chem. Biol.* **2016**, *23*, 849–861.

(37) Erburu, M.; Muñoz-Cobo, I.; Diaz-Perdigon, T.; Mellini, P.; Suzuki, T.; Puerta, E.; Tordera, R. M. SIRT2 inhibition modulate glutamate and serotonin systems in the prefrontal cortex and induces antidepressant-like action. *Neuropharmacology* **2017**, *117*, 195–208.

(38) Song, N.-Y.; Surh, Y.-J. Janus-faced role of SIRT1 in tumorigenesis. *Ann. N. Y. Acad. Sci.* **2012**, *1271*, 10–19.

(39) Liu, T.; Liu, P. Y.; Marshall, G. M. The critical role of the class III histone deacetylase SIRT1 in cancer. *Cancer Res.* **2009**, *69*, 1702–1705.

(40) Roth, M.; Chen, W. Y. Sorting out functions of sirtuins in cancer. *Oncogene* **2014**, *33*, 1609–1620.

(41) Chalkiadaki, A.; Guarente, L. The multifaceted functions of sirtuins in cancer. *Nat. Rev. Cancer* **2015**, *15*, 608–624.

(42) Wu, X.; Cao, N.; Fenech, M.; Wang, X. Role of sirtuins in maintenance of genomic stability: relevance to cancer and healthy aging. *DNA Cell Biol.* **2016**, *35*, 542–575.

(43) Wu, W.; Zhang, L.; Lin, J.; Huang, H.; Shi, B.; Lin, X.; Huang, Z.; Wang, C.; Qiu, J.; Wei, X. Hypermethylation of the HIC1 promoter and aberrant expression of HIC1/SIRT1 contribute to the development of thyroid papillary carcinoma. *Oncotarget* **2016**, *7*, 84416–84427.

(44) Tseng, R.-C.; Lee, C.-C.; Hsu, H.-S.; Tzao, C.; Wang, Y.-C. Distinct HIC1-SIRT1-p53 loop deregulation in lung squamous carcinoma and adenocarcinoma patients. *Neoplasia N. Y. N* **2009**, *11*, 763–770.

(45) Yamakuchi, M.; Ferlito, M.; Lowenstein, C. J. miR-34a repression of SIRT1 regulates apoptosis. *Proc. Natl. Acad. Sci. U. S. A.* **2008**, *105*, 13421–13426.

(46) Lim, J.-H.; Lee, Y.-M.; Chun, Y.-S.; Chen, J.; Kim, J.-E.; Park, J.-W. Sirtuin 1 modulates cellular responses to hypoxia by deacetylating hypoxia-inducible factor 1α. *Mol. Cell* **2010**, *38*, 864–878.

(47) Kim, H.-S.; Vassilopoulos, A.; Wang, R.-H.; Lahusen, T.; Xiao, Z.; Xu, X.; Li, C.; Veenstra, T. D.; Li, B.; Yu, H.; Ji, J.; Wang, X. W.; Park, S.-H.; Cha, Y. I.; Gius, D.; Deng, C.-X. SIRT2 maintains genome integrity and suppresses tumorigenesis through regulating APC/C activity. *Cancer Cell* **2011**, *20*, 487–499.

(48) Dan, L.; Klimenkova, O.; Klimiankou, M.; Klusman, J.-H.; van den Heuvel-Eibrink, M. M.; Reinhardt, D.; Welte, K.; Skokowa, J. The role of sirtuin 2 activation by nicotinamide phosphoribosyltransferase in the aberrant proliferation and survival of myeloid leukemia cells. *Haematologica* **2012**, *97*, 551–559.

(49) Deng, A.; Ning, Q.; Zhou, L.; Liang, Y. SIRT2 is an unfavorable prognostic biomarker in patients with acute myeloid leukemia. *Sci. Rep.* **2016**, *6*, 27694.

(50) Hou, H.; Chen, W.; Zhao, L.; Zuo, Q.; Zhang, G.; Zhang, X.; Wang, H.; Gong, H.; Li, X.; Wang, M.; Wang, Y.; Li, X. Cortactin is associated with tumour progression and poor prognosis in prostate cancer and SIRT2 other than HADC6 may work as facilitator in situ. *J. Clin. Pathol.* **2012**, *65*, 1088–1096.

(51) Liu, P. Y.; Xu, N.; Malyukova, A.; Scarlett, C. J.; Sun, Y. T.; Zhang, X. D.; Ling, D.; Su, S.-P.; Nelson, C.; Chang, D. K.; Koach, J.; Tee, A. E.; Haber, M.; Norris, M. D.; Toon, C.; Rooman, I.; Xue, C.; Cheung, B. B.; Kumar, S.; Marshall, G. M.; Biankin, A. V.; Liu, T. The histone deacetylase SIRT2 stabilizes Myc oncoproteins. *Cell Death Differ.* **2013**, *20*, 503–514.

(52) Kozako, T.; Suzuki, T.; Yoshimitsu, M.; Arima, N.; Honda, S.; Soeda, S. Anticancer agents targeted to sirtuins. *Molecules* **2014**, *19*, 20295–202313.

(53) Carafa, V.; Rotili, D.; Forgione, M.; Cuomo, F.; Serretiello, E.; Hailu, G. S.; Jarho, E.; Lahtela-Kakkonen, M.; Mai, A.; Altucci, L. Sirtuin functions and modulation: from chemistry to the clinic. *Clin. Epigenetics* **2016**, *8*, 61.

(54) Yoshida, M.; Kudo, N.; Kosono, S.; Ito, A. Chemical and structural biology of protein lysine deacetylases. *Proc. Jpn. Acad. Ser. B Phys. Biol. Sci.* **2017**, *93*,5 297–321.

(55) Rotili, D.; Tarantino, D.; Nebbioso, A.; Paolini, C.; Huidobro, C.; Lara, E.; Mellini, P.; Lenoci, A.; Pezzi, R.; Botta, G.; Lahtela-Kakkonen, M.; Poso, A.; Steinkühler, C.; Gallinari, P.; De Maria, R.; Fraga, M.; Esteller, M.; Altucci, L.; Mai, A. Discovery of salermide-related sirtuin inhibitors: binding mode studies and antiproliferative effects in cancer cells including cancer stem cells. *J. Med. Chem.* **2012**, *55*, 10937–10947.

(56) McCarthy, A. R.; Pirrie, L.; Hollick, J. J.; Ronseaux, S.; Campbell, J.; Higgins, M.; Staples, O. D.; Tran, F.; Slawin, A. M. Z.; Lain, S.; Westwood, N. J. Synthesis and biological characterisation of sirtuin inhibitors based on the tenovins. *Bioorg. Med. Chem.* **2012**, *20*, 1779–1793.

(57) Li, L.; Wang, L.; Li, L.; Wang, Z.; Ho, Y.; McDonald, T.; Holyoake, T. L.; Chen, W.; Bhatia, R. Activation of p53 by SIRT1 inhibition enhances elimination of CML leukemia stem cells in combination with imatinib. *Cancer Cell* **2012**, *21*, 266–281.

(58) Zhang, Y.; Au, Q.; Zhang, M.; Barber, J. R.; Ng, S. C.; Zhang, B. Identification of a small molecule SIRT2 inhibitor with selective tumor cytotoxicity. *Biochem. Biophys. Res. Commun.* **2009**, *386*, 729–733.

(59) Fridén-Saxin, M.; Seifert, T.; Landergren, M. R.; Suuronen, T.; Lahtela-Kakkonen, M.; Jarho, E. M.; Luthman, K. synthesis and evaluation of substituted chroman-4-one and chromone derivatives as sirtuin 2-selective inhibitors. *J. Med. Chem.* **2012**, *55*, 7104–7113.

(60) Seifert, T.; Malo, M.; Kokkola, T.; Engen, K.; Fridén-Saxin, M.; Wallén, E. A. A.; Lahtela-Kakkonen, M.; Jarho, E. M.; Luthman, K. Chroman-4-one- and chromone-based sirtuin 2 inhibitors with antiproliferative properties in cancer cells. *J. Med. Chem.* **2014**, *57*, 9870–9888.

(61) Suzuki, T.; Khan, M. N. A.; Sawada, H.; Imai, E.; Itoh, Y.; Yamatsuta, K.; Tokuda, N.; Takeuchi, J.; Seko, T.; Nakagawa, H.; Miyata, N. Design, synthesis, and biological activity of a novel series of human sirtuin-2-selective inhibitors. *J. Med. Chem.* **2012**, *55*, 5760–5773.

(62) Tatum, P. R.; Sawada, H.; Ota, Y.; Itoh, Y.; Zhan, P.; Ieda, N.; Nakagawa, H.; Miyata, N.; Suzuki, T. Identification of novel SIRT2-selective inhibitors using a click chemistry approach. *Bioorg. Med. Chem Lett.* **2014**, *24*, 1871–1874.

(63) Moniot, S.; Forgione, M.; Lucidi, A.; Hailu, G. S.; Nebbioso, A.; Carafa, V.; Baratta, F.; Altucci, L.; Giacché, N.; Passeri, D.; Pellicciari, R.; Mai, A.; Steegborn, C.; Rotili, D. Development of 1,2,4-oxadiazoles as potent and selective inhibitors of the human deacetylase sirtuin 2: structure–activity relationship, X-ray crystal structure, and anticancer activity. *J. Med. Chem.* **2017**, *60*, 2344–2360.

(64) Sundriyal, S.; Moniot, S.; Mahmud, Z.; Yao, S.; Di Fruscia, P.; Reynolds, C. R.; Dexter, D. T.; Sternberg, M. J. E.; Lam, E. W.-F.; Steegborn, C.; Fuchter, M. J. Thienopyrimidinone based sirtuin-2 (SIRT2)-selective inhibitors bind in the ligand induced selectivity pocket. *J. Med. Chem.* **2017**, *60*, 1928–1945.

(65) Shah, A. A.; Ito, A.; Nakata, A.; Yoshida, M. Identification of a selective SIRT2 inhibitor and its anti-breast cancer activity. *Biol. Pharm. Bull.* **2016**, *39*, 1739–1742.

(66) Kudo, N.; Ito, A.; Arata, M.; Nakata, A.; Yoshida, M. Identification of a novel small molecule that inhibits deacetylase but not defatty-acylase reaction catalysed by SIRT2. *Philos. Trans. R. Soc. B* **2018**, *373*, 20170070.

(67) Rumpf, T.; Schiedel, M.; Karaman, B.; Roessler, C.; North, B. J.; Lehotzky, A.; Oláh, J.; Ladwein, K. I.; Schmidtkunz, K.; Gajer, M.; Pannek, M.; Steegborn, C.; Sinclair, D. A.; Gerhardt, S.; Ovádi, J.; Schutkowski, M.; Sippl, W.; Einsle, O.; Jung, M. Selective sirt2 inhibition by ligand-induced rearrangement of the active site. *Nat. Commun.* **2015**, *6*, 6263.

(68) Swyter, S.; Schiedel, M.; Monaldi, D.; Szunyogh, S.; Lehotzky, A.; Rumpf, T.; Ovádi, J.; Sippl, W.; Jung, M. New chemical tools for probing activity and inhibition of the NAD^+-dependent lysine deacylase sirtuin 2. *Phil. Trans. R. Soc. B* **2018**, *373*, 20170083.

(69) Schiedel, M.; Herp, D.; Hammelmann, S.; Swyter, S.; Lehotzky, A.; Robaa, D.; Oláh, J.; Ovádi, J.; Sippl, W.; Jung, M. Chemically induced degradation of sirtuin 2 (Sirt2) by a proteolysis targeting chimera (PROTAC) based on sirtuin rearranging ligands (SirReals). *J. Med. Chem.* **2018**, *61*, 482–491.

(70) Schiedel, M.; Rumpf, T.; Karaman, B.; Lehotzky, A.; Oláh, J.; Gerhardt, S.; Ovádi, J.; Sippl, W.; Einsle, O.; Jung, M. Aminothiazoles as potent and selective Sirt2 inhibitors: a structure-activity relationship study. *J. Med. Chem.* **2016**, *59*, 1599–1612.

(71) Schiedel, M.; Rumpf, T.; Karaman, B.; Lehotzky, A.; Gerhardt, S.; Ovádi, J.; Sippl, W.; Einsle, O.; Jung, M. Structure-based development of an affinity probe for sirtuin 2. *Angew. Chem. Int. Ed. Engl.* **2016**, *55*, 2252–2256.

(72) Robaa, D.; Monaldi, D.; Wössner, N.; Kudo, N.; Rumpf, T.; Schiedel, M.; Yoshida, M.; Jung, M. Opening the selectivity pocket in the human lysine deacetylase sirtuin2 - new opportunities, new questions. *Chem. Rec.* **2018**, *18*, 1701–1707.

(73) Jing, H.; Hu, J.; He, B.; Negrón Abril, Y. L.; Stupinski, J.; Weiser, K.; Carbonaro, M.; Chiang, Y.-L.; Southard, T.; Giannakakou, P.; Giannakakou, P.; Weiss, R. S.; Lin, H. A SIRT2-selective inhibitor promotes c-Myc oncoprotein degradation and exhibits broad anticancer activity. *Cancer Cell* **2016**, *29*, 297–310.

(74) Li, Y.; Zhang, M.; Dorfman, R. G.; Pan, Y.; Tang, D.; Xu, L.; Zhao, Z.; Zhou, Q.; Zhou, L.; Wang, Y.; Yin, Y.; Shen, S.; Kong, B.; Friess, H.; Zhao, S.; Wang, L.; Zou, X. SIRT2 promotes the migration and invasion of gastric cancer through RAS/ERK/JNK/MMP-9 pathway by increasing PEPCK1-related metabolism. *Neoplasia* **2018**, *20*, 745–756.

(75) Mellini, P.; Itoh, Y.; Tsumoto, H.; Li, Y.; Suzuki, M.; Tokuda, N.; Kakizawa, T.; Miura, Y.; Takeuchi, J.; Lahtela-Kakkonen, M.; Suzuki, T. Potent mechanism-based sirtuin-2-selective inhibition by an *in situ*-generated occupant of the substrate-binding site, "selectivity pocket" and NAD^+-binding site. *Chem. Sci.* **2017**, *8*, 6400–6408.

(76) Delorme, D.; Woo, S. H.; Vaisburg A. Preparation of Hydroxamic Acids as Inhibitors of Histone Deacetylase. PCT Int. Appl., 2001070675, 2001.

(77) Kalluraya, B.; Lingappa, B.; Nooji, S. R. Synthesis and biological study of some novel 4-[5-(4,6-disubstituted-2-thiomethylpyrimidyl)-4'-amino-1,2,4-triazol-3'-yl] thioacetyl-3-arylsydnones. *Phosphorus Sulfur Silicon Relat. Elem.* **2007**, *182*, 1393–1401.

(78) El-Faham, A.; Subirós Funosas, R.; Prohens, R.; Albericio, F. COMU: a safer and more effective replacement for benzotriazole-based uronium coupling reagents. *Chem. Eur. J.* **2009**, *15*, 9404–9416.

(79) He, B.; Du, J.; Lin, H. Thiosuccinyl peptides as Sirt5-specific inhibitors. *J. Am. Chem. Soc.* **2012**, *134*, 1922–1925.

(80) Nicolaou, K. C.; Estrada, A. A.; Zak, M.; Lee, S. H.; Safina, B. S. A mild and selective method for the hydrolysis of esters with trimethyltin hydroxide. *Angew. Chem. Int. Ed. Engl.* **2005**, *44*, 1378–1382.

(81) Pettersen, E. F.; Goddard, T. D.; Huang, C. C.; Couch, G. S.; Greenblatt, D. M.; Meng, E. C.; Ferrin, T. E. UCSF chimera-a visualization system for exploratory research and analysis. *J. Comput. Chem.* **2004**, *25*, 1605–1612.

(82) Itoh, Y.; Suzuki, M.; Matsui, T.; Ota, Y.; Hui, Z.; Tsubaki, K.; Suzuki, T. False HDAC inhibition by aurone compound. *Chem. Pharm. Bull.* **2016**, *64*, 1124–1128.

(83) Miyake, Y.; Itoh, Y.; Hatanaka, A.; Suzuma, Y.; Suzuki, M.; Kodama, H.; Arai, Y.; Suzuki, T. Identification of novel lysine demethylase 5-selective inhibitors by inhibitor-based fragment merging strategy. *Bioorg. Med. Chem.* **2019**, *27*, 1119–1129.

(84) North, B. J.; Marshall, B. L.; Borra, M. T.; Denu, J. M.; Verdin, E. The human Sir2 ortholog, SIRT2, is an NAD^+-dependent tubulin deacetylase. *Mol. Cell* **2003**, *11*, 437–444.

(85) Kalle, A. M.; Mallika, A.; Badiger, J.; Alinakhi; Talukdar, P.; Sachchidanand. Inhibition of SIRT1 by a small molecule induces apoptosis in breast cancer cells. *Biochem. Biophys. Res. Commun.* **2010**, *401*, 13–19.

(86) Vaquero, A.; Scher, M.; Lee, D.; Erdjument-Bromage, H.; Tempst, P.; Reinberg, D. Human SirT1 interacts with histone H1 and promotes formation of facultative heterochromatin. *Mol. Cell.* **2004**, *16*, 93–105.

(87) Feng, Y.; Liu, T.; Dong, S. Y.; Guo, Y. J.; Jankovic, J.; Xu, H.; Wu, Y. C. Rotenone affects p53 transcriptional activity and apoptosis via targeting SIRT1 and H3K9 acetylation in SH-SY5Y cells. *J. Neurochem.* **2015**, *134*, 668–676.

(88) Kaur, N.; Zhou, B.; Breitbeil, F.; Hardy, K.; Kraft, K. S.; Trantcheva, I.; Phanstiel, O. A delineation of diketopiperazine self-assembly processes: understanding the molecular events involved in N^{ε}-(fumaroyl)diketopiperazine of $_{L}$-Lys (FDKP) interactions. *Mol. Pharm.* **2008**, *5*, 294–315.

(89) Uchida, S.; Hara, K.; Kobayashi, A.; Otsuki, K.; Yamagata, H.; Hobara, T.; Suzuki, T.; Miyata, N.; Watanabe, Y. Epigenetic status of Gdnf in the ventral striatum determines susceptibility and adaptation to daily stressful events. *Neuron* **2011**, *69*, 359–372.

(90) Howitz, K. T.; Zhang, Z.; Kisielewski, A.; Dale, E.; Patton, W. F. Preparation of Fluorogenic Substrates for Detection of Sirtuin and Histone Deacetylase. PCT Int. Appl., WO2012096800, 2012.

Table of Contents Graphic